Chapter 5

Electron interactions for radiation damage modelling of aqua DNA constituents

In this study we have investigated the interactions of electrons with the DNA constituents in their aqueous phase in order to obtain the quantities useful for DNA damage assessment. We have computed various electron collision cross-sections, inelastic mean free path (IMFP), mass stopping power (MSP) and absorbed dose (D) for the DNA constituents (Adenine, Cytosine, Guanine, Thymine and Uracil) in the aqueous medium from ionization threshold to 5000 eV. We have modified complex optical potential formalism to include band gap of the systems to calculate inelastic cross sections which are used to estimate these entities. This is the maiden attempt to report these important quantities for the aqueous DNA constituents. We have compared our results with available data in gas or condensed phase and have observed explicable accord. Also, this is the first attempt to report the absorbed dose values for these molecules. Since these are the first results of absorbed dose (D) for these compounds, we have explored present results vis-a-vis dose absorption in water.

5.1 Introduction

The genetic code in all living things is created by the double-stranded helical macromolecule DNA. This sequence's integrity must be preserved for the cell to continue to function normally and to replicate, and any errors or damage could lead to carcinogenesis and cell death [1,2]. DNA molecules are assumed to be the biological tissues that are most vulnerable

to radiation. Ionizing radiation exposure to DNA species causes a variety of DNA damage [3]. It is very common for ionising radiation to be used in the realm of medicine. It is extensively used as a therapeutic agent and a probe in the field of radio diagnostics in the medical industry. It is crucial to simulate both primary and secondary species' paths across a biological medium because they cause radiation damage when ionising radiation interacts with cell molecules. This enables foresight and comprehension of the kind, location, and degree of cell injury. The charged-particle track structures show the path that the primary and secondary particles take as they travel through the medium [4]. These aleatory (stochastic) simulations use the cross-section values to model the whole range of interactions between the primary and secondary species at the level of each atom or molecule. Hence, the validity of these kinds of simulations depends on precise values of cross-sections.

The study of the energy deposited by electrons in DNA and the damage they cause is a major focus of radiation dosimetry [5]. Two distinguishing factors, Inelastic Mean Free Path (IMFP) and Stopping Power (SP), can be used to quantify the average energy deposited in the inelastic events as a result of ionised particles [6]. They are crucial when employing the Monte Carlo method to study electron transport through solids and liquids [7,8]. Basic research in both radiation biology and biomedical applications significantly rely on IMFP and SP [6].

Many studies have been published thus far on the effects of electrons on DNA constituents in their gaseous, solid, or condensed phases [4–8]. However, taking into account the DNA's aqueous phase rather than its gaseous or condensed phase offers a more realistic perspective because they are always found covered in water molecules via hydrogen bonding. The specific structure of the DNA is actually determined by the number of H_2O molecules that surround it [9,10].

Thus, for this case, we have determined different inelastic and elastic cross-sections for the aqueous building blocks of DNA—Adenine, Guanine, Thymine, Cytosine, and Uracil. Also, for each of these DNA components, we have determined the inelastic mean free path (IMFP), mass stopping power (MSP), and absorbed dose (D), all of which are important measurements for the assessment of DNA damage.

5.2 Various cross-sections

When the main ionising particle enters the biological medium, multiple collision mechanisms, such as excitations and ionisations, cause it to deposit the majority of its energy. This high energy transfer results in a significant release of secondary electrons, and these electrons can interact with a number of biological materials, resulting in radiation damage. So, in order to mimic the cell damage, it is imperative to trace their courses across a biological media. This enables foresight and comprehension of the kind, location, and degree of cell injury. The charged-particle track structures show the path that the primary and secondary particles take as they travel through the medium [4]. These aleatory (stochastic) simulations use the cross-section values to model the whole range of interactions between the primary and secondary species at the level of each atom or molecule. Hence, the validity of these kinds of simulations depends on accurate cross-sections. Hence, the present work reports data on the elastic, total, ionisation, and inelastic cross sections for all of the aqueous DNA constituents under study.

5.2.1 Literature survey and Molecular properties

The literature data for the present investigation are displayed in Table 5.1. Since there are no data available for DNA molecule calculations in the aqueous phase, we have compared our findings to those for DNA molecules in the condensed phase.

Table 5.1 Literature survey

Sr. No.	Quantity	Energy range (eV)	Theoretical Method	References
1	Q_{inel}	20-10000	Dielectric response theory	Tan *et.al.* [11]
2	Q_{ion}	10-500		Tan *et.al.* [12]
3		1-10000		Vera *et.al.* [13]

Various target properties which have been used in the computations are listed in table 5.2.

Table 5.2 Molecular characteristics

Target	Aqueous phase IE (eV)	Energy band gap (E_{gap}) in eV
Adenine	5.00 [14,15]	5.25 [16]
Cytosine	5.50 [14,15]	5.35 [17]

Guanine	4.80 [14,15]	4.80 [18]
Thymine	5.40 [14,15]	5.20 [19]
Uracil	5.55 [14]	5.70 [17]

5.2.2 Results and discussion

A. Inelastic processes

Q_{inel} and Q_{ion} for the present investigated DNA constituents are shown in figures 1-5 as a function of the electron energy, along with the results of Tan *et.al.* [11], Vera *et.al.* [13] and Tan *et.al.* [12].

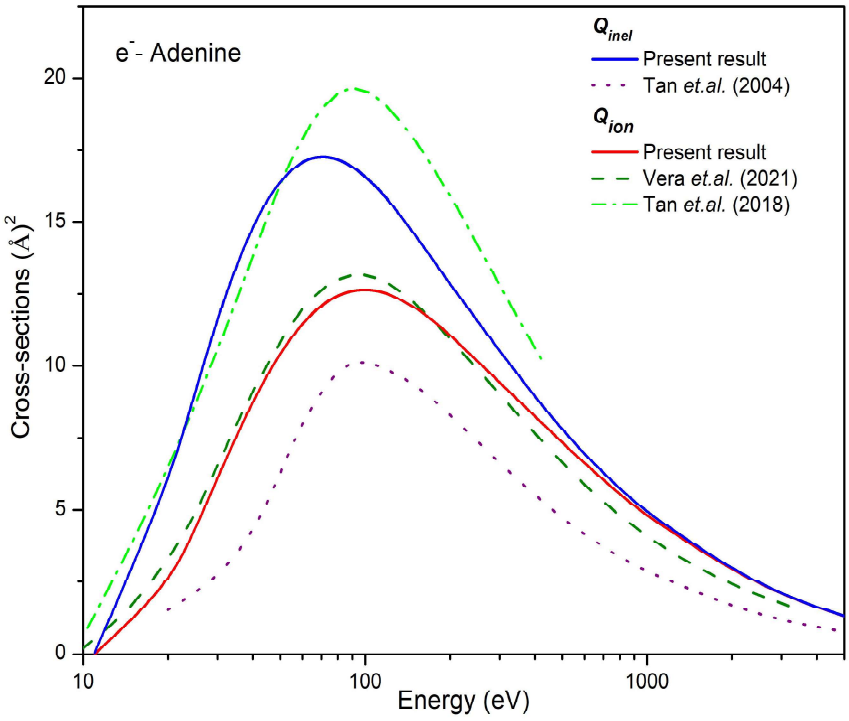

Figure 5.1 Inelastic interaction CSs for Adenine

Blue solid: Present Q_{inel}; dot: Tan et.al. Q_{inel} [11]*; red solid: Present Q_{ion}; dash: Vera et.al. Q_{ion}* [13]*; dash dot: Tan et.al. Q_{ion}* [12]

The Q_{ion} results for condensed DNA bases have been provided by Tan *et.al.* [12] and Vera *et.al.* [13] using the approaches that underlines the dielectric response theory. Except in the case of Uracil, the current results of Q_{ion} are seen to be in excellent agreement with those of

Vera *et.al.* [13]. Consideration of the various phases for the molecules may account for the minuscule deviation at the highest value of Q_{ion}.

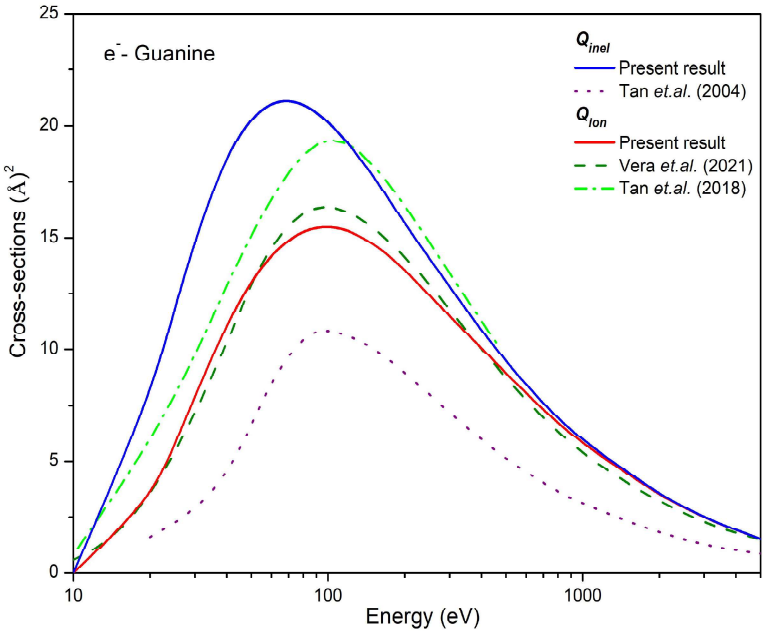

Figure 5.2 Inelastic interaction CSs for Guanine

Blue solid: Present Q_{inel}; dot: Tan et.al. Q_{inel} [11]*; red solid: Present Q_{ion}; dash: Vera et.al. Q_{ion}* [13]*; dash dot: Tan et.al. Q_{ion}* [12]

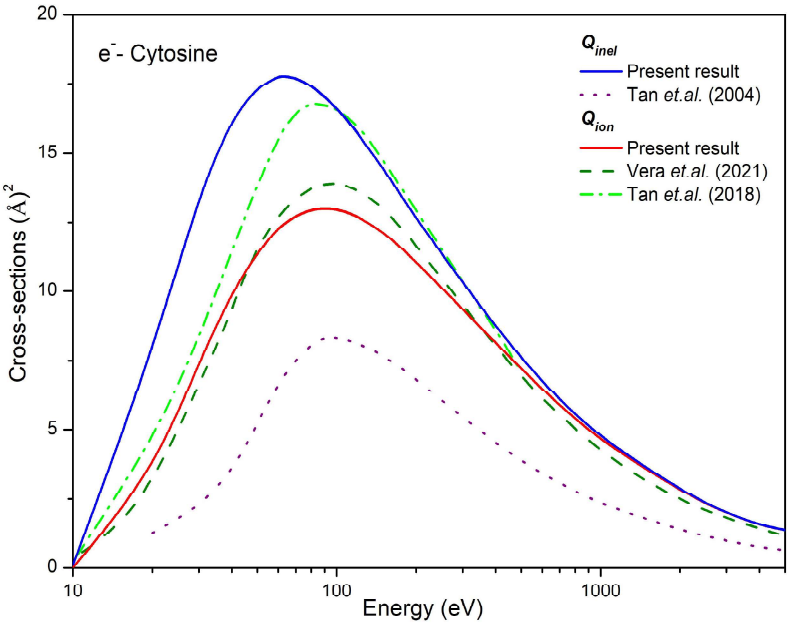

Figure 5.3 Inelastic interaction CSs for Cytosine

Blue solid: Present Q_{inel}; dot: Tan et.al. Q_{inel} [11]*; red solid: Present Q_{ion};*

dash: Vera et.al. Q_{ion} [13]*; dash dot: Tan et.al. Q_{ion}* [12]

Apart from Thymine, the data from Tan *et.al.* [12] overestimate both the current data and those from Vera *et.al.* [13]. Tan *et.al.* [11] used Penn's approximation and the dielectric response theory to provide the Q_{inel} data for the case of DNA in water. They divided an identical DNA molecule, which included 50% Guanine-Cytosine and 50% Adenine-Thymine in a water environment, into its five constituent DNA molecules. Yet, their Q_{inel} have extremely low values even when compared to the existing Q_{ion} results for molecules in the condensed phase, which is unexpected.

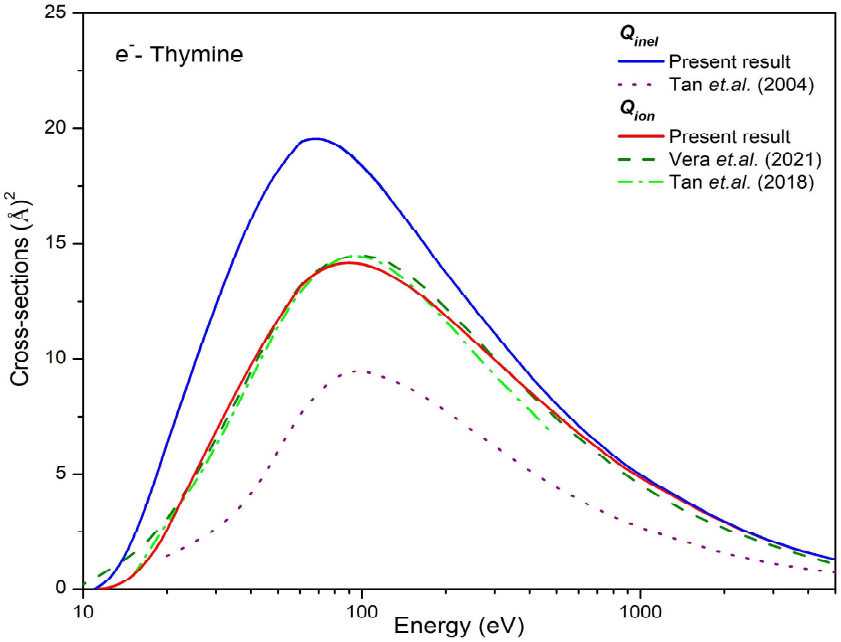

Figure 5.4 Inelastic interaction CSs for Thymine

Blue solid: Present Q_{inel}; dot: Tan et.al. Q_{inel} [11]*; red solid: Present Q_{ion}; dash: Vera et.al. Q_{ion}* [13]*; dash dot: Tan et.al. Q_{ion}* [12]

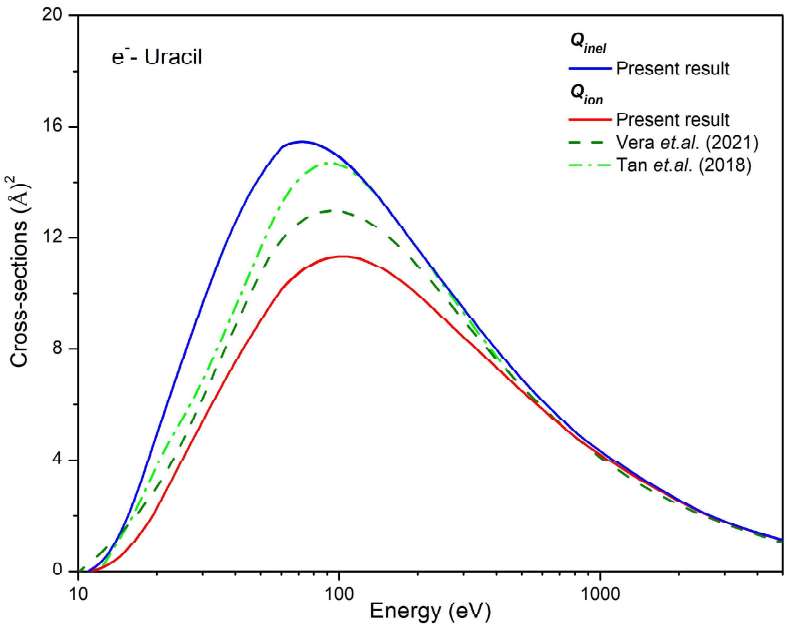

Figure 5.5 Inelastic interaction CSs for Uracil

Blue solid: Present Q_{inel}; dot: Tan et.al. Q_{inel} [11]*; red solid: Present Q_{ion}; dash: Vera et.al. Q_{ion}* [13]*; dash dot: Tan et.al. Q_{ion}* [12]

B. Elastic processes

We have estimated the elastic CSs (Q_{el}) and then the total CSs (Q_T) for the electron energies from molecular *IE* to 5000 eV using the predicted polarizability values for all the aqueous DNA nucleobases. Figures 5.6 to 5.10 show the Q_{el} and Q_T graphs for aqueous adenine, cytosine, guanine, thymine, and uracil against incident electron energies.

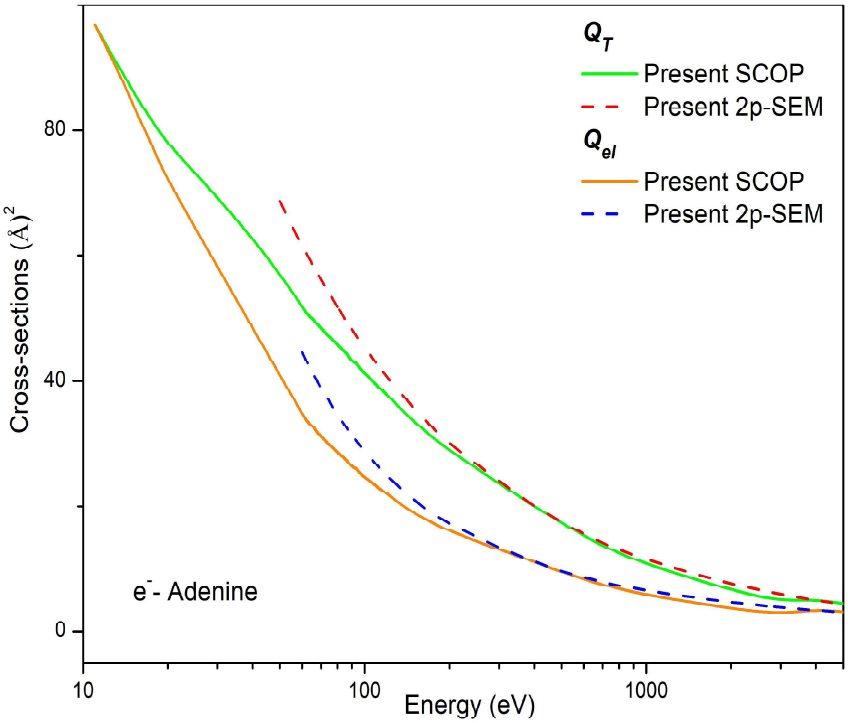

Figure 5.6 Elastic interaction CSs for Adenine

Green solid: Present SCOP Q_T; red dash: Present 2p-SEM Q_T; orange solid: Present SCOP Q_{el}; blue dash: Present 2p-SEM Q_{el}

The proposed 2p-SEM approximation (described in the theory section) has been used to compute the Q_T for all of the studied species over the energy range of 50–10000 eV. The results from the optical complex potential formalism and the 2p-SEM are observed to be in good agreement.

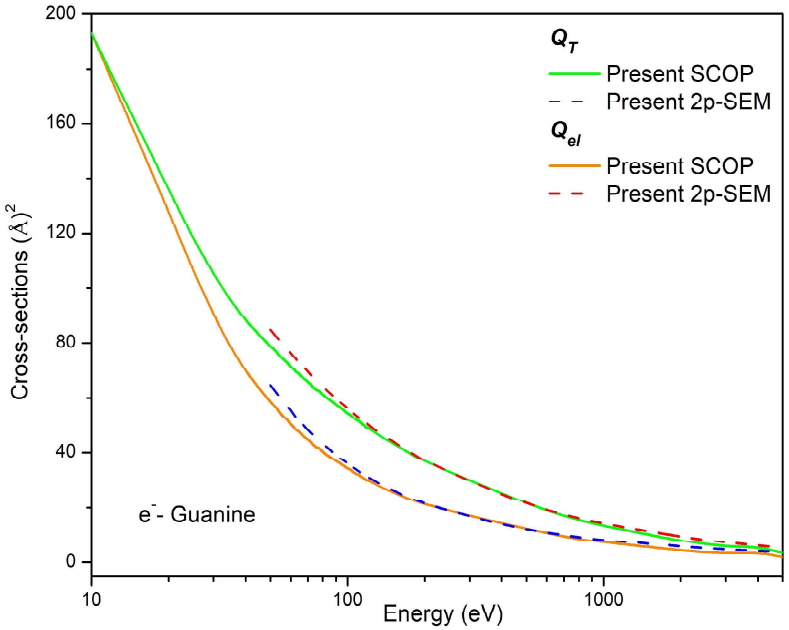

Figure 5.7 Elastic interaction CSs for Guanine

Green solid: Present SCOP Q_T; red dash: Present 2p-SEM Q_T; orange solid: Present SCOP Q_{el}; blue dash: Present 2p-SEM Q_{el}

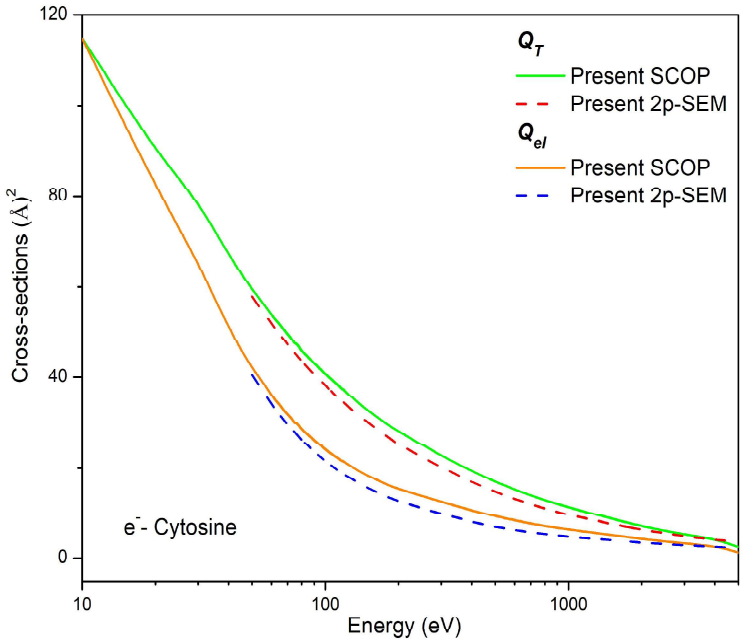

Figure 5.8 Elastic interaction CSs for Cytosine

Green solid: Present SCOP Q_T; red dash: Present 2p-SEM Q_T; orange solid: Present SCOP Q_{el}; blue dash: Present 2p-SEM Q_{el}

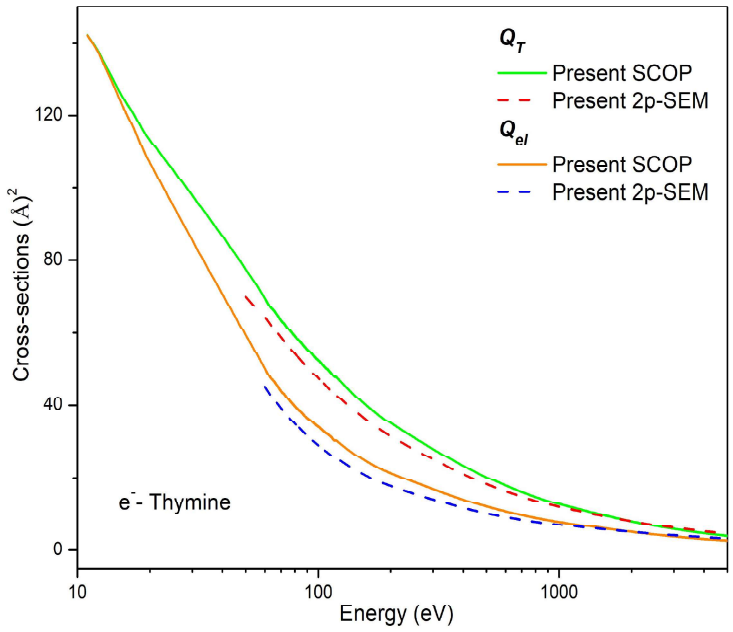

Figure 5.9 Elastic interaction CSs for Thymine

Green solid: Present SCOP Q_T; red dash: Present 2p-SEM Q_T; orange solid: Present SCOP Q_{el}; blue dash: Present 2p-SEM Q_{el}

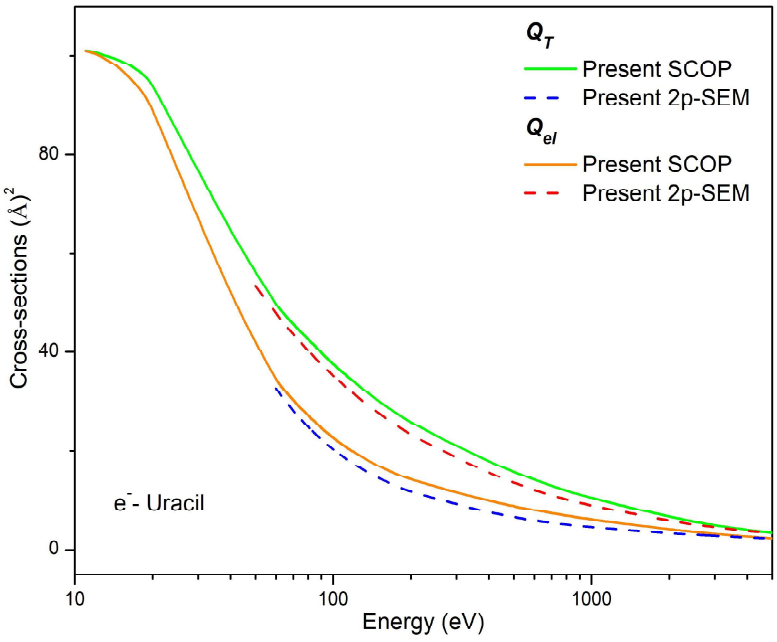

Figure 5.10 Elastic interaction CSs for Uracil

Green solid: Present SCOP Q_T; red dash: Present 2p-SEM Q_T; orange solid: Present SCOP Q_{el}; blue dash: Present 2p-SEM Q_{el}

After computing the Q_T from 2p-SEM, we utilised those Q_T results to obtain the Q_{el}, by subtracting the Q_{inel} data produced through optical complex potential approach from the Q_T results of 2p-SEM. The Q_{el} results from both the methodologies (2p-SEM and optical complex potential approach) are observed to be in good accord with each other for all the present studied molecules.

We used the Q_T results derived from the 2p-SEM to calculate the Q_{el}, by deducting the Q_{inel} data computed by the optical complex potential technique from the Q_T results of the 2p-SEM. For all of the currently under study compounds, it is seen that the Q_{el} values from the two techniques (2p-SEM and SCOP) are in good agreement with one another.

C. Various correlations: Prediction of molecular characteristics

Here, we have explored various correlations between cross-sections and target properties which leads to estimate the molecular polarizability and dielectric constant.

Molecular polarisability

According to Harland's proposed qualitative dependency nature of the maximum ionisation CSs, (Q_{ion} (peak)) with its polarisability (α) [20],

$$Q_{ion\,(peak)} = \frac{e}{4\varepsilon_o}\sqrt{\frac{\alpha}{\Delta}} \tag{5.1}$$

Harland proposed the Δ will be equal to *IE* in case of gas phase of the target system. While, in the present case of aqueous phase species, the $\Delta = IE + E_{gap}$, and the ionisation of the system actually occurs when the incoming energy is greater than the threshold value, Δ = *IE* + E_{gap}.

Using this equation 5.1, we have predicted the α values for the present studied targets as given in the Table 5.3,

Table 5.3 Predicted polarisability α (Å^3)

Target	Δ (eV)	Q_{ion} (peak) (Å^2)	Predicted α (Å^3)	Reference value of α for condensed phase (Å^3) [21]
Adenine	10.25	12.65	11.54	14.33
Guanine	9.60	15.47	16.17	15.26

Thymine	10.60	14.17	14.99	13.35
Cytosine	10.85	12.99	12.88	11.47
Uracil	11.25	11.32	10.15	10.41

From the table it can be observed that the present predicted α for the aqueous molecules find good agreement with those of Nakagawa [21], who calculated the α for condensed molecules.

Dielectric constant (ε)

The two expressions for dielectric constant (ε) have been derived in the present work using the dependency of the Q_{ion}(peak) on α and ε (equation 2.63 and 2.65). The first proposed expression of dielectric constant as a function of Q_{ion} (peak), derived using the dependency of Q_{ion} (peak) with α (equation 5.1) and the Clausius-Mosotti (CM) equation,

$$\frac{\varepsilon-1}{\varepsilon+2} = C \cdot \left(Q_{ion\ (peak)}\right)^2 N\Delta \tag{5.2}$$

where, C is the constant = $\frac{64\pi}{3}\left(\frac{\varepsilon_o}{e}\right)^2$ and N is the number density of the molecule.

Secondly, the Onsager dielectric equation [22,23], which works well for the case of liquids is given by,

$$\frac{\varepsilon-1}{\varepsilon+2} = \frac{4\pi}{3}\alpha N + \frac{(\varepsilon-\varepsilon_\infty)(2\varepsilon+\varepsilon_\infty)}{\varepsilon(\varepsilon_\infty+2)^2} \tag{5.3}$$

This equation is thought to be more applicable in the present aqueous phase study, and again the equation of dielectric constant as a function of Q_{ion} (peak) is proposed as,

$$\frac{\varepsilon-1}{\varepsilon+2} = C \cdot \left(Q_{ion\ (peak)}\right)^2 N\Delta + \frac{(\varepsilon-\varepsilon_\infty)(2\varepsilon+\varepsilon_\infty)}{\varepsilon(\varepsilon_\infty+2)^2} \tag{5.4}$$

where, ε_∞ is the high frequency dielectric constant, which can be obtained from the CM equation. The computed ε values are listed in Table 5.4.

Table 5.4 Computed dielectric constants (ε)

Target	**Q_{ion} (peak) (Å^2)**	**Dielectric constant (ε) (vide equation 5.3)**	**Dielectric constant (ε) (vide equation 5.4)**	**Reference value of ε for condensed phase** [24]
Adenine	12.65	2.22	1.00	1.59
Guanine	15.47	3.23	0.85	1.77
Thymine	14.17	3.39	0.99	1.59

Cytosine	12.99	2.84	1.03	1.71
Uracil	11.32	2.29	0.98	-

Form the table 5, it can be observed as expected that the ε values computed through equation 13, are in good agreement with those of Szarek [24].

5.3 Inelastic Mean Free Path (IMFP)

Inelastic mean free path (IMFP) is the average distance a charged particle travels within a medium between two subsequent inelastic collisions. Radiation biology track-structure computations use this IMFP data as their primary input [25–28]. The inelastic mean free path for electrons with energies below 1000 eV must be precisely understood in order to perform radiation dosimetry and scanning electron spectroscopies [29]. Also, it is crucial when utilising the Monte Carlo method to model electron transport through solids and liquids [7,8]. Both basic research in radiation biology and related biomedical applications primarily rely on IMFP [6]. Hence, by taking into account their aqueous phase, we provided the IMFP for the energies, ionisation threshold to 5000 eV, for the current five DNA compounds.

5.3.1 Molecular properties and Literature study

Table 5.5 contains a list of the molecular properties used in the calculations of IMFP for the electron interactions with DNA constituents, viz., Adenine, Cytosine, Guanine, Thymine and Uracil.

Table 5.5 Molecular parameters

Target	**Aqueous phase *IE* (eV)**	**Band gap E_{gap} (eV)**	**Target density, ρ (gm/cm^3)**	**Molar mass, *M* (gm/mol)**
Adenine	5.00 [14,15]	5.25 [16]	1.35 [30]	135.14 [30]
Cytosine	5.50 [14,15]	5.35 [17]	1.30 [30]	111.11 [30]
Guanine	4.80 [14,15]	4.80 [18]	1.58 [30]	151.14 [30]
Thymine	5.40 [14,15]	5.20 [19]	1.48 [30]	126.12 [30]
Uracil	5.55 [14]	5.70 [17]	1.32 [30]	112.09 [30]

Table 5.6 shows the literature study on the electron IMFP for all the DNA constituents. All of the existing results of IMFP for DNA compounds has been computed by considering their condensed or solid phase. Present study is the first effort to compute IMFP for aqueous phase DNA molecules.

Table 5.6 Literature study on IMFP of DNA constituents

Target	Energy range (eV)	Method of investigation	References
Adenine ($C_5H_5N_5$)	50-2000	Dielectric response theory and Penn's statistical approximation	Tanuma *et.al.* [31]
	20-1000000	Generalized oscillator strength (GOS) model	Akar *et.al.* [32]
	200-2000	Quantitative structure–property relationship (QSPR) scheme	Cumpson *et.al.* [33]
	20-10000	Dielectric response theory and Penn's statistical approximation	Tan *et.al.* [6,30,34]
	11-1000000	Geant4-DNA model	Zein *et.al.* [35]
Cytosine ($C_4H_5N_3O$)	20-1000000	Generalized oscillator strength (GOS) model	Akar *et.al.* [32]
	20-10000	Dielectric response theory and Penn's statistical approximation	Tan *et.al.* [34]
	11-1000000	Geant4-DNA model	Zein *et.al.* [35]
Guanine ($C_5H_5N_5O$)	50-2000	Dielectric response theory and Penn's statistical approximation	Tanuma *et.al.* [31]
	20-1000000	Generalized oscillator strength (GOS) model	Akar *et.al.* [32]
	200-2000	Quantitative structure–property relationship (QSPR) scheme	Cumpson *et.al.* [33]
	20-10000	Dielectric response theory (experimental OELF fitted by a sum of Drude type functions)	Akkerman and Akkerman [36]
	20-10000	Dielectric response theory and Penn's statistical approximation	Tan *et.al.* [6,30,34]
	11-1000000	Geant4-DNA model	Zein *et.al.* [35]
Thymine ($C_5H_6N_2O_2$)	20-10000	Dielectric response theory and Penn's statistical approximation	Tan *et.al.* [34]
	11-1000000	Geant4-DNA model	Zein *et.al.* [35]
	20-1000000	Generalized oscillator strength (GOS) model	Akar *et.al.* [32]

Uracil ($C_4H_4N_2O_2$)	20-10000	Dielectric response theory and Penn's statistical approximation	Tan *et.al.* [34]

5.3.2 Results and Discussion

In figures 5.11 to 5.15, we have shown the IMFP for aqueous Adenine, Cytosine, Guanine, Thymine and Uracil, respectively. The shape of the IMFP curve is explained by inelastic cross-sections (Q_{inel}). The average distance that electron travels within the medium between successive collisions is at its greatest at the ionisation threshold. As the energy goes up, there are more collisions and the IMFP goes down.

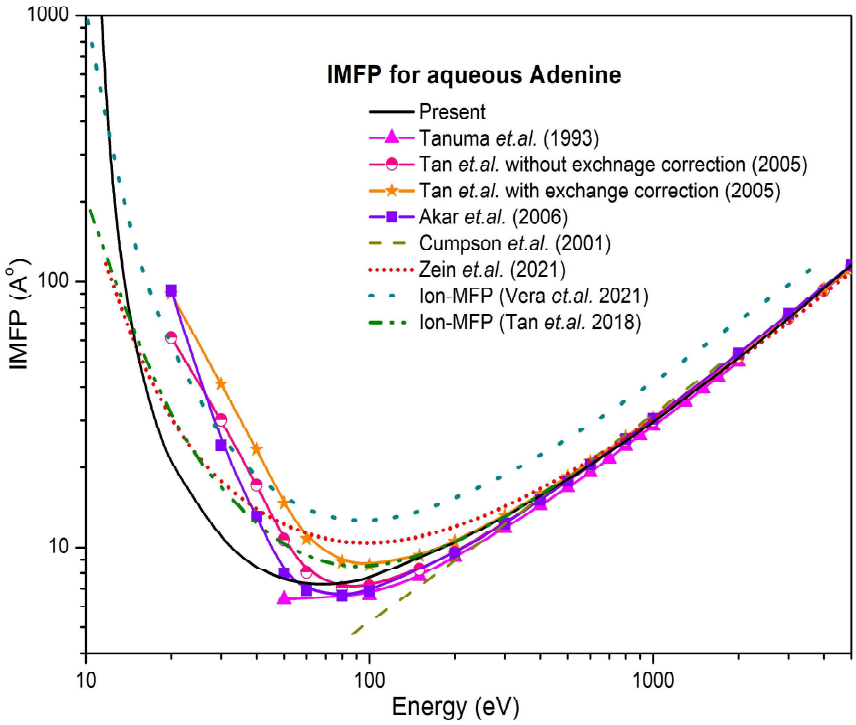

Figure 5.11 IMFP for aqueous Adenine

Line: Present; Filled triangles: Tanuma et. al. [31]*; half-filled circles: Tan et. al. without exchange* [30]*; filled stars: Tan et. al. with Born-Ochkur* [30]*; filled squares: Akar et. al.* [32]*; dash line: Cumpson et. al.* [33]*; short dot line: Zein et. al.* [35]*; dot line: Ion-MFP from Vera et. al.* [13]*; dash dot dot line: Ion-MFP from Tan et. al.* [12]

Further, at an energy of 80–90 eV, the peak of the Q_{inel} is reached, which shows that the average distance travelled in this energy region is at its lowest. As energy goes beyond 100 eV, electrons have less time to collide with molecules, resulting in a decrease in Q_{inel} and an increase in IMFP values from its valley region.

The present IMFP data as shown in figure 5.11 are in good accord with the results obtained using optical energy loss function (OELF) followed by Penn's statistical approach by Tan *et.al.* [30], and Tanuma *et.al.* [31], with those results of Akar *et.al.* [32] utilising Generalized Oscillator strength (GOS) model for the electron energy higher than 70 eV and with those results of Cumpson *et.al.* [33] using Quantitative Structure-Property relationships (QSPR). The present curve starts to converge with all of the data as the impact energy rises. The results of Tanuma *et.al.* [31] and Tan *et.al.* [30] differ from the present values for below 50 eV energy, because they employed Penn's algorithm, which is more applicable for energies beyond 50 eV [37]. Moreover, for energy below 200 eV, IMFP values derived from optical data are less accurate [31,33]. In their methodology, which deals with the approximation of free electron gas on the assumption that the energy-momentum relation for a non-relativistic electron in solid is similar to that of a free electron in vacuum, Tan *et.al.* [30] used the Linhard dielectric function in OELF calculation and also included the exchange correction of Born-Ochkur. Thus, the present IMFP obtained by taking their aqueous phase in to account are more realistic. The first-Born approximation, which is more accurate at higher energies, is used to generate the IMFP data from the GOS model computation by Akar *et.al.* [32]. As a result, their data is likewise thought to be less credible than the present ones at lower energy regime. According to Cumpson *et.al.* [33], the IMFP values were reported using QSPR relationships, and the optical data of Tanuma *et.al.* [31] were utilised to fit the IMFP equation accurately for the energy range of 200–2000 eV. For energies below 300 eV, the present data overstates those of Cumpson *et.al.* [33], and for higher energies, it begins to merge. The Geant4-DNA code simulation results [35] are higher in the valley region but exhibit a similar pattern to the present one.

Figures 5.11 to 5.15 show a comparison between the present IMFP, and the ionisation mean free path (Ion-MFP) computed by us from the ionisation CSs data of Vera *et.al.* [13] and Tan *et.al.* [12] for condensed DNA constituents. The Ion-MFP data for all molecules overstate the present IMFP curve, which is expected as the current IMFP involves all of the inelastic interaction events (excitations and ionizations), as can be seen in figures 5.11 to 5.15.

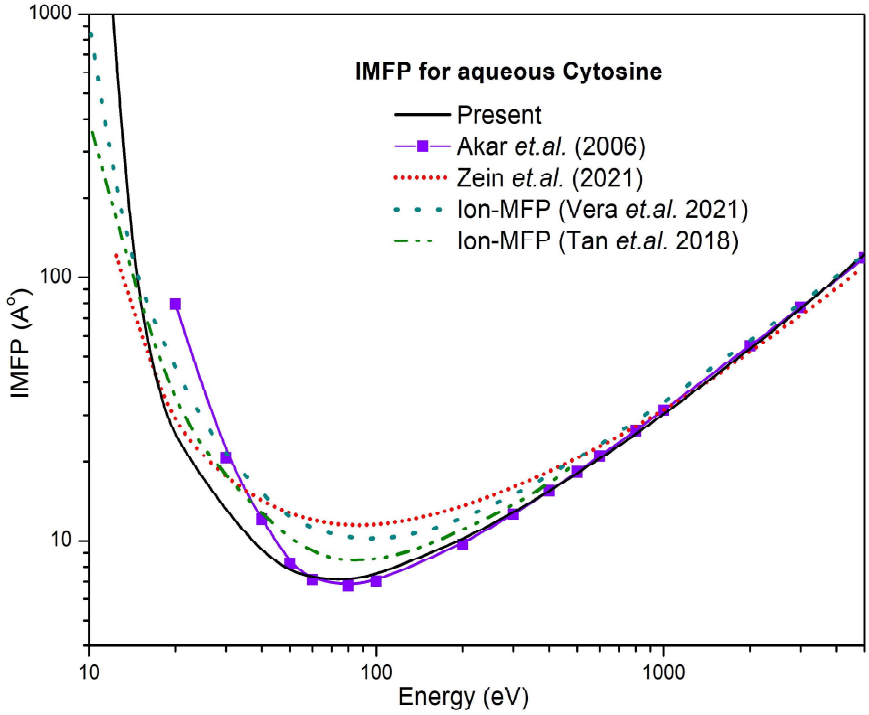

Figure 5.12 IMFP for aqueous Cytosine

Line: Present; filled squares: Akar et.al. [32]*; short dot line: Zein et.al.* [35]*; dot line: Ion-MFP from Vera et.al.* [13]*; dash dot dot line: Ion-MFP from Tan et.al.* [12]

Figure 5.12 depicts the IMFP results of the Cytosine molecule. The IMFP results for this target were only reported by Akar *et.al.* [32] and Zein *et.al.* [35]. The divergence of Akar *et.al.* [32] data from the present values is noticed here again for energy E < 50 eV due to the same causes as in the case of Adenine, whereas for the rest of the energy range (E > 50 eV) the present data overlaps with them. The present values are in good accord with the data of Zein *et.al.* [35] derived from the Geant4-DNA code, with the exception of the valley region, where they underestimate.

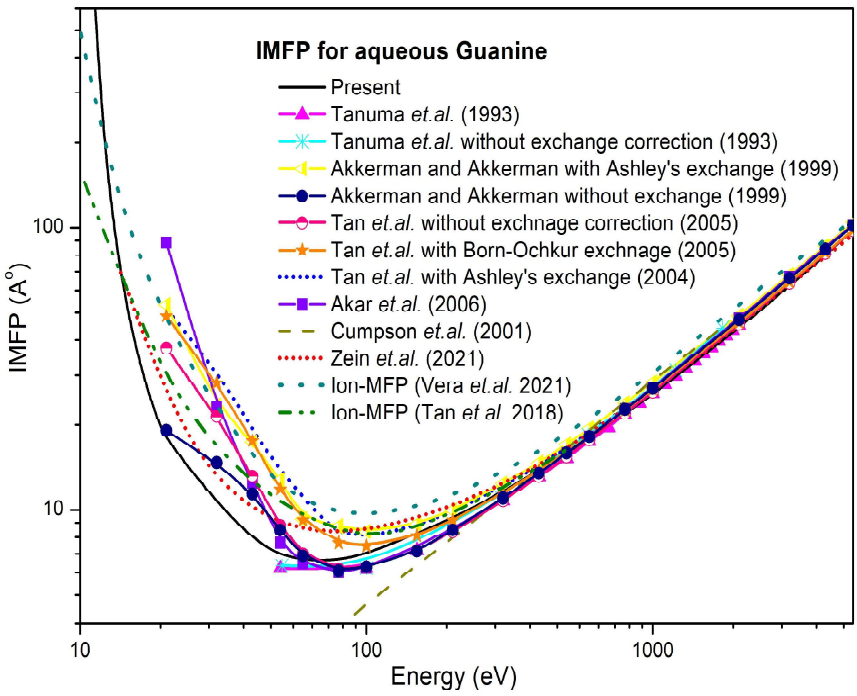

Figure 5.13 IMFP for aqueous Guanine

Line: Present; filled triangles: Tanuma et.al. [31]*; asterisk: Tanuma et.al. without exchange* [31]*; half-filled triangles: Akkerman and Akkerman with Ashley exchange* [36]*; solid circles: Akkerman and Akkerman without exchange* [36]*; half-filled circles: Tan et.al. without exchange* [30]*; filled stars: Tan et.al. with Born-Ochkur exchange* [30]*; short blue dot: Tan et.al. with Ashley exchange* [34]*; filled squares: Akar et.al.* [32]*; dark yellow dash line: Cumpson et.al.* [33]*; short red dot: Zein et.al.* [35]*; dot line: Ion-MFP from Vera et.al.* [13]*; dash dot dot line: Ion-MFP from Tan et.al.* [12]

The IMFP plot for the most studied target, the Guanine molecule, is shown in Figure 5.13. Because of the reasons described above, the current IMFP curve has similar behaviour to Tanuma *et.al.* [31], Tan *et.al.* [30], Akar *et.al.* [32], Cumpson *et.al.* [33] and Zein *et.al.* [35]. At energies E > 70 eV, there is a good match between the current results and those of Tan *et.al.* without exchange correction [30], Tanuma *et.al.* [31], and Akar *et.al.* [32]. Beyond 70 eV, the results of Akkerman and Akkerman [36] are observed to be in good agreement with the current data. They calculated the IMFP and SP values for the Guanine molecule by fitting the experimental energy loss function (ELF) with a sum of Drude-type functions. At energies

less than 50 eV, there is a disagreement between their [36] results and the present one. The argument given by them is that the accuracy of their data is inferior since the approximated treatment of exchange effect may raise the probable inaccuracies in IMFP and SP calculations by up to 100% [36]. In this case, too, the current curve understates the Zein *et.al.* [35] data in the valley region before merging in the higher energy zone.

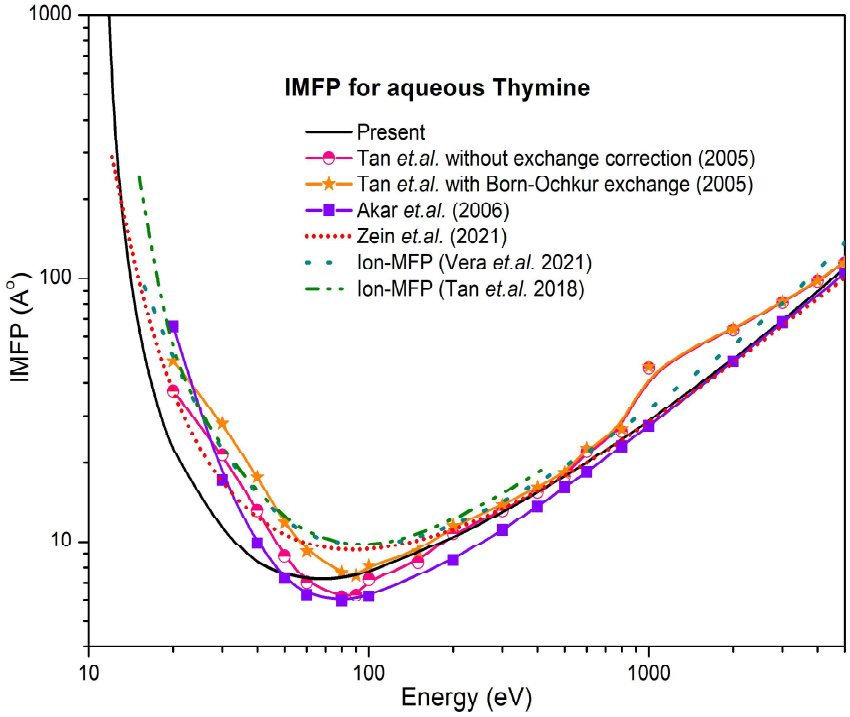

Figure 5.14 IMFP for aqueous Thymine

Line: Present; half-filled circles: Tan et.al. without exchange [30]*; filled stars: Tan et.al. with Born-Ochkur exchange* [30]*; filled squares: Akar et.al.* [32]*; short red dot: Zein et.al.* [35]*; dot line: Ion-MFP from Vera et.al.* [13]*; dash dot dot line: Ion-MFP from Tan et.al.* [12]

Figure 5.14 depicts the electron IMFP for Thymine. There is a fair agreement between the present values of IMFP and the results of Tan *et.al.* [30] can be seen. They begin to overlap at energies higher than 150 eV. The data of Akar *et.al.* [32] is found to be lower than the present ones in the valley region, but they match well at higher energies. A similar pattern to that seen in earlier examples by Zein *et.al.* [35] is observed here as well.

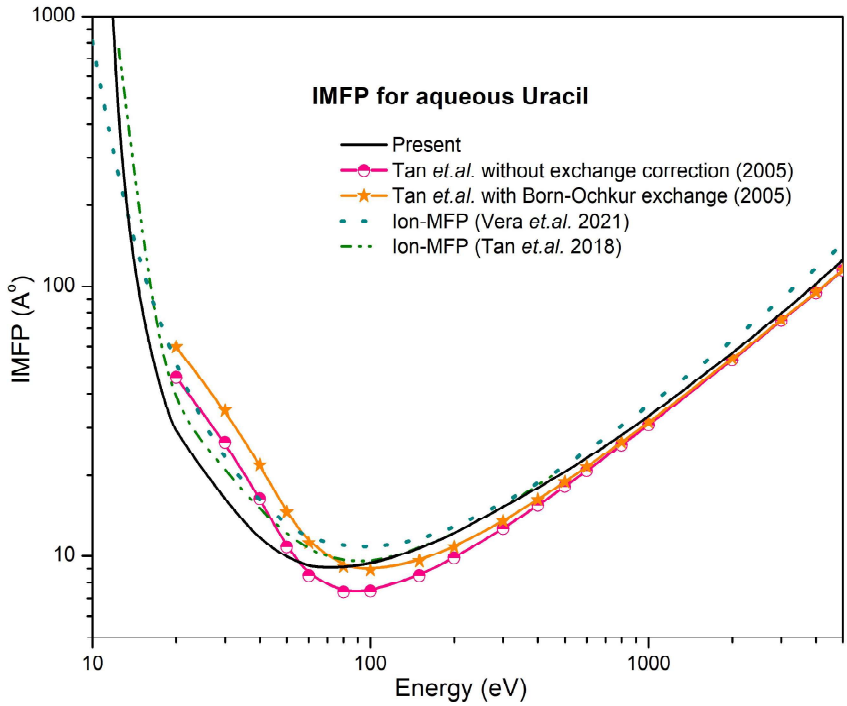

Figure 5.15 IMFP for aqueous Uracil

Line: Present; half-filled circles: Tan et.al. without exchange [30]*; filled stars: Tan et.al. with Born-Ochkur exchange* [30]*; dot line: Ion-MFP from Vera et.al.* [13]*; dash dot dot line: Ion-MFP from Tan et.al.* [12]

Figure 5.15 shows the case of the Uracil molecule. Tan *et.al.* [30] were the only authors to report the IMFP values for this target, without and with Born-Ochkur exchange correction. The current findings are in good agreement with their data [30].

Figure 5.16 compares the current IMFP results for aqueous DNA constituents to those of Nidhi Sinha and Bobby Antony [38] and those of Emfietzoglou *et.al.* [39] for liquid water.

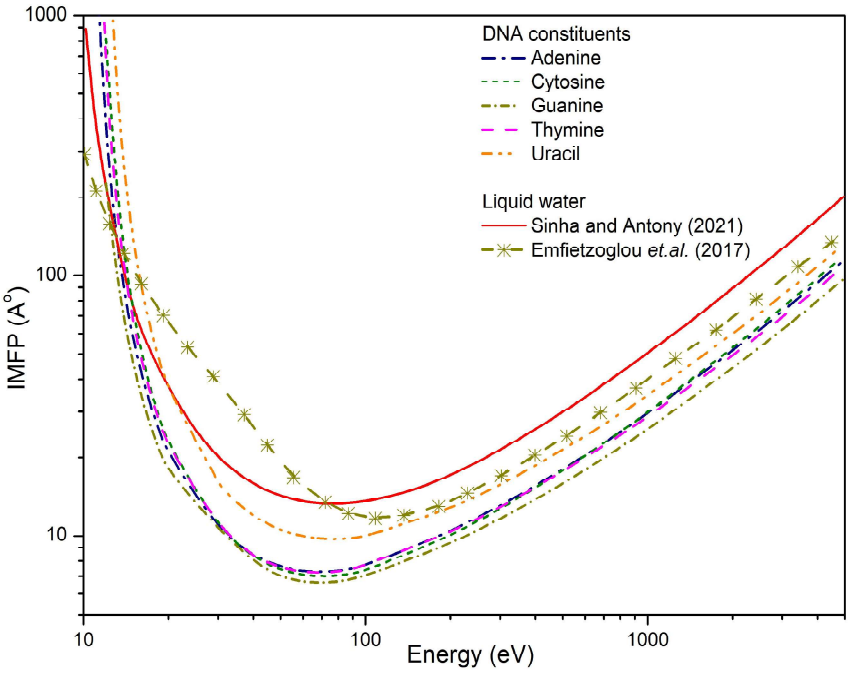

Figure 5.16 IMFP of DNA molecules and liquid water

Line: liquid water from Nidhi Sinha and Bobby Antony [38]*; asterisk: liquid water from Emfietzoglou et.al.* [39]

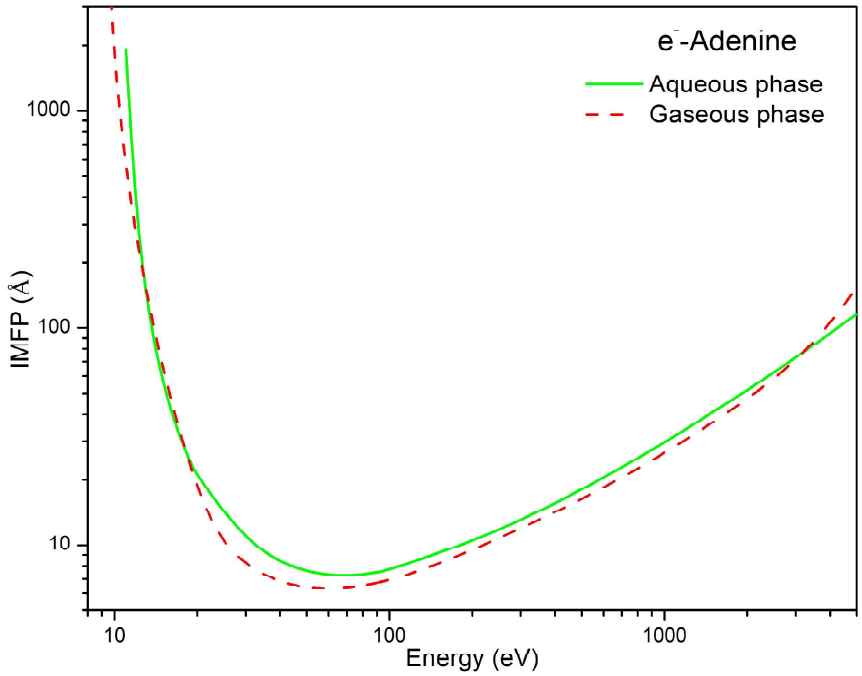

Figure 5.17 IMFP for gaseous Adenine and aqueous Adenine

Figures 5.17 to 5.21 provide a comparison of the IMFP results of aqueous and gaseous DNA components. The computations for both phases were completed only using the current methods. The inclusion of the energy band gap is omitted in gaseous phase calculations since a valance electron is ejected in the free phase of the molecule when the incident electron energy is $E_i \geq IE$.

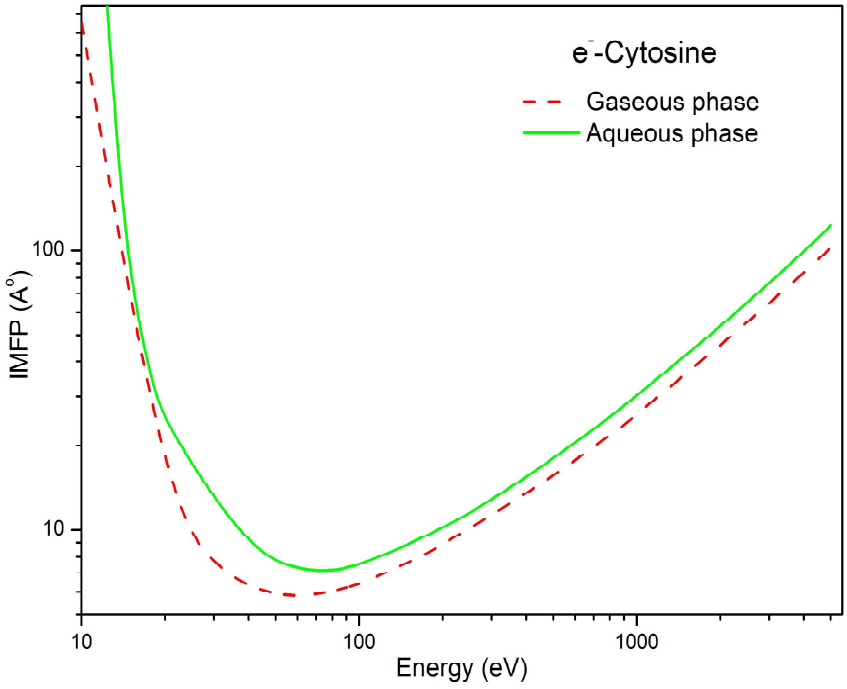

Figure 5.18 IMFP for gaseous Cytosine and aqueous Cytosine

Figures 5.17 to 5.21 show that the IMFP values for gaseous phase molecules are lower than those for aqueous phase molecules. This is because Q_{inel} are more sensitive to ionisation energy and have a high value at peak energy (around 80-100 eV) in their gas phase compared to their aqueous phase.

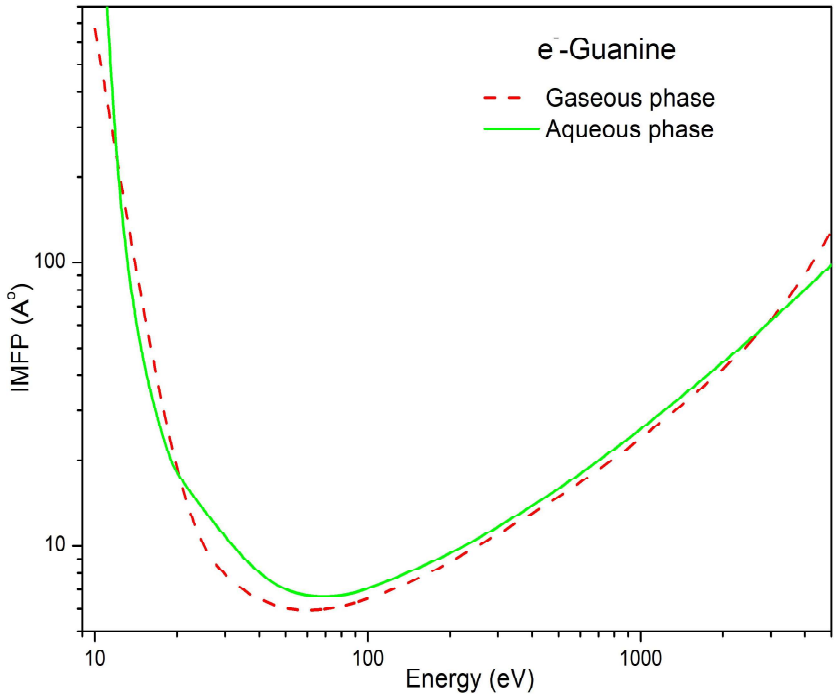

Figure 5.19 IMFP for gaseous Guanine and aqueous Guanine

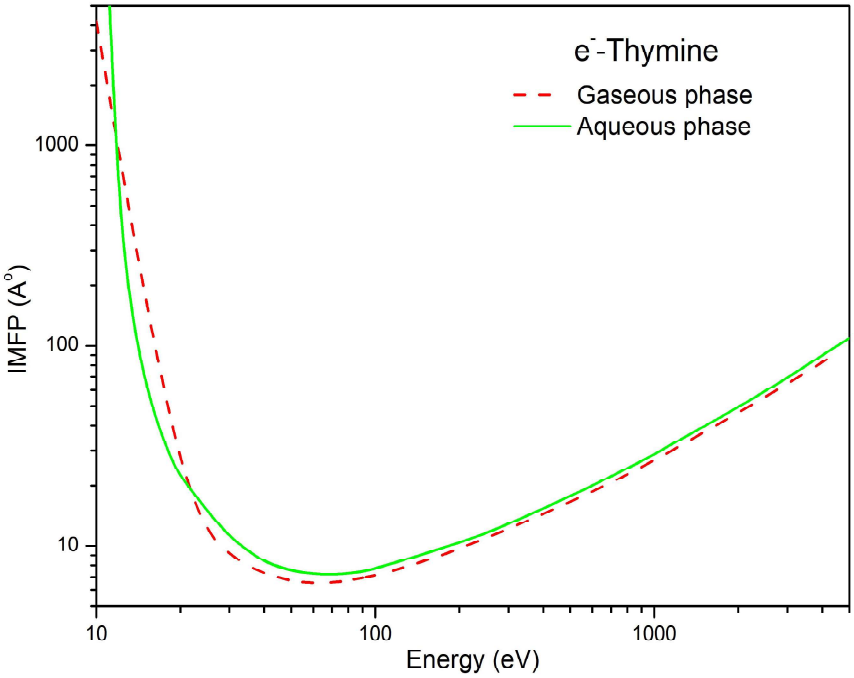

Figure 5.20 IMFP for gaseous Thymine and aqueous Thymine

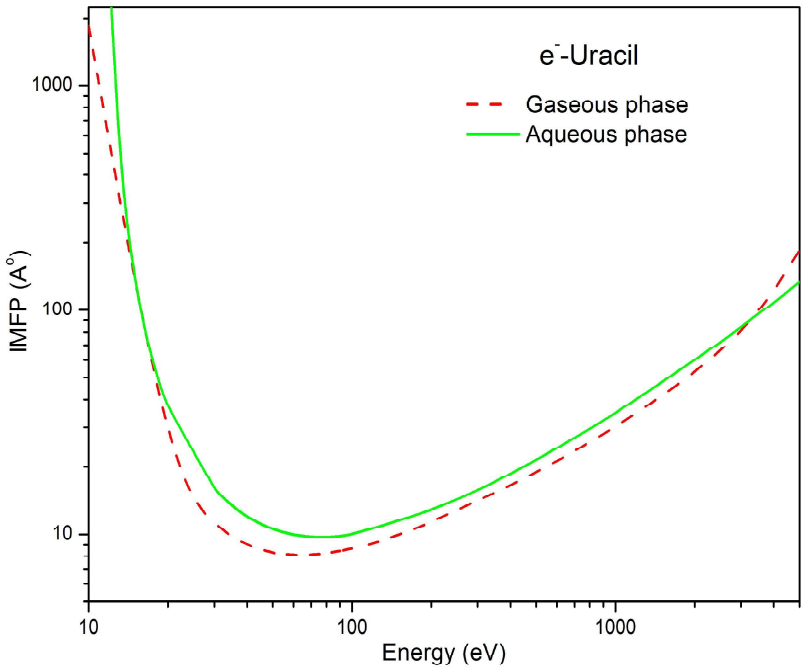

Figure 5.21 IMFP for gaseous Uracil and aqueous Uracil

5.4 Mass Stopping Power (MSP)

The average energy dissipated by a charged particle is an important statistic for analysing radiation impact in medical and environmental applications [40] and is known as Stopping Power (SP) [41]. It is commonly employed in Monte Carlo simulations of electron transport in biomaterials [6,42], but it can also be used to estimate dose or other relevant parameters without relying on comprehensive calculations for electron transport [43]. To account for the density of the target molecule, we provided the mass stopping power (MSP) for all aqueous DNA nucleobases in this work.

5.4.1 Literature survey and Molecular properties

Stopping power (SP) have been previously calculated by Tan *et.al.* [6,30,34], Tanuma *et.al.* [31], Akkerman and Akkerman [36], and Jablonski *et.al.* [44] based on the dielectric response theory, followed by the evaluation of optical energy loss function (OELF) through

different methods. Theoretical methods like generalized oscillator strength (GOS) model by Akar and Gümüş [32,45,46], Quantitative structure–property relationship (QSPR) scheme by Cumpson *et.al.* [33], Geant4 DNA simulations [35], SP calculation from Modified Rohrlich and Carlson formula by Gümüş and Bentabet [47], Rudd model calculation by Francis *et.al.* [48], Predictive S-lamda expression by Jablonski *et.al.* [44], the expressions of Joy and Luo [49] and that of Fernandez-Varea *et.al.* [50] are employed for such study. Most of these theoretical and semi-empirical approaches are not suitable for low energy calculations, but they are good at higher energy regime [6,30–34,36,44,45]. The present theory employs partial wave calculations which provide reliable results even at low energy side. With the use of single quantum mechanical approach, current methodology allows us to estimate overall probability of all the molecular processes into the inelastic channel and compute macroscopic entities such as IMFP, MSP and absorbed dose (D) for aqueous phase molecules. It uses the properties of the material (table 5.5 and 5.7) and electronic charge density to adequately describe the (n+1) interactions (see theory section).

The mean excitation energies of the DNA constituents, which have been used for the computations of MSP are listed in table 5.7.

Table 5.7 Mean excitation energies of the target

Target	**Mean excitation energy, $\overline{E}$ (eV)** [52]
Adenine	56.23
Cytosine	57.19
Guanine	58.37
Thymine	57.44
Uracil	59.91

5.4.2 Results and Discussion

In this subsection, we present our results on MSP for DNA constituents in aqueous medium, as seen in figures 5.22 to 5.26, along with accessible comparisons. The energy loss per unit length caused by successive inelastic collisions between electrons and molecules is referred to as stopping power. However, for the present examined molecules, we have computed the

MSP, as it is a more essential quantity because it involves the density of the medium through which the electron energy loss occurs. The energy loss is reduced for low energy due to the lower probability of inelastic collisions. The energy loss is greatest at the peak value of Q_{inel}, resulting in the maximum value of MSP. With higher incident particle energies, the interaction time reduces, resulting in less energy loss and a receding MSP.

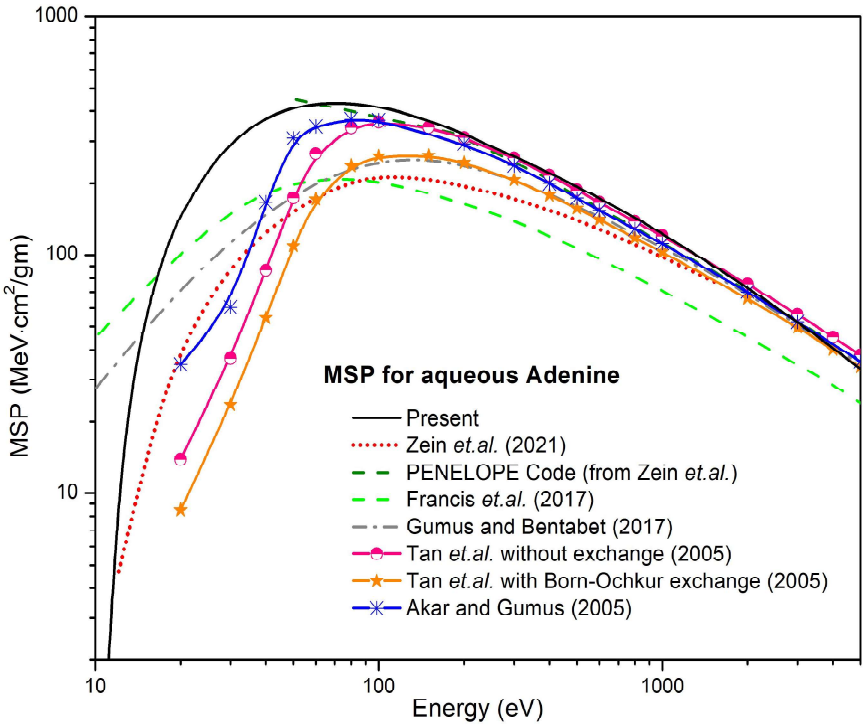

Figure 5.22 MSP for aqueous Adenine

Line: Present; short red dot: Zein et.al. [35]; olive green dash line: PENELOPE code [35]; green dash line: Francis et.al. [48]; gray dash dot: Gümüş and Bentabet [47]; half-filled circles: Tan et.al. without exchange [30]; filled stars: Tan et.al. with Born-Ochkur exchange [30]; asterisk: Akar and Gümüş [45]

Figure 5.22 shows the current MSP data for aqueous Adenine as well as the available comparison. As shown in the figure, there are differences across all available data in the lower energy domain. For energies greater than 50 eV, the present MSP values show excellent matching with Tan *et.al*. data without exchange [30], Akar and Gümüş [45] results and PENELOPE code simulation [35] data. Tan *et.al.* [30] also reported the data using Born-Ochkur exchange correction. Francis *et.al.* [48] and Tan *et.al.* [30] reported stopping power (SP) values (in eV/Å), which were then converted into mass stopping power, MSP

(MeV·cm^2/gm) by us using the presently reported density values (table 5.5) for the specific target. The Born-Ochkur formalism-based DCSs produce a bit lower collision stopping powers, around a few hundred eV, which causes electron tracks to spread out in all directions [53]. Tan *et.al.* [30] data with Born-Ochkur correction hence underestimates the present MSP results. Francis *et.al.* [48] calculated differential cross-sections using the Rudd model, which provide values within ±10-20% uncertainty, and then entered those DCS into the Geant4-DNA class to calculate the SP. Their findings underestimate all existing data, including current ones, for energies beyond 70 eV. Gümüş and Bentabet [47] provided MSP values for the energy 10-10^7 eV by expanding the semi-empirical model [54,55] to produce MSP data for gaseous bioorganic molecules, whereas the present data deals with the molecule's aqueous phase. As a result, the difference between their data and the present values can be understood. The present curve overestimates Zein *et.al.* [35] data.

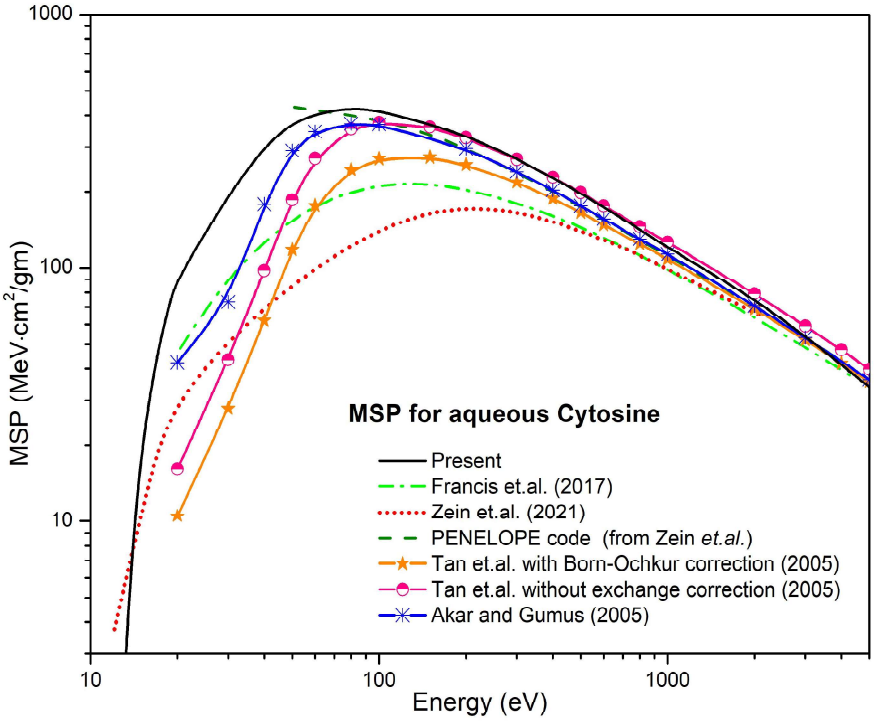

Figure 5.23 MSP for aqueous Cytosine

Line: Present; dash line: Francis et.al. [48]; short dot line: Zein et.al. [35]; olive green dash line: PENELOPE code [35]; half-filled circles: Tan et.al. without exchange [30]; filled stars: Tan et.al. with Born-Ochkur [30]; asterisk: Akar and Gümüş [45]

Figure 5.23 illustrates the case of mass stopping power of aqueous cytosine. All of the data for energies less than 600 eV show deviation [30,35,45,48] with respect to each other. For energies above 70 eV, the present values are in excellent agreement with Tan *et.al.* data without exchange correction [30], Akar and Gümüş [45] values and PENELOPE code simulation [35] results. As previously noted, Tan *et.al.* [30] data with Born-Ochkur exchange produce lower SP values, however Francis *et.al.* [48] data are uncertained by 10-20%.

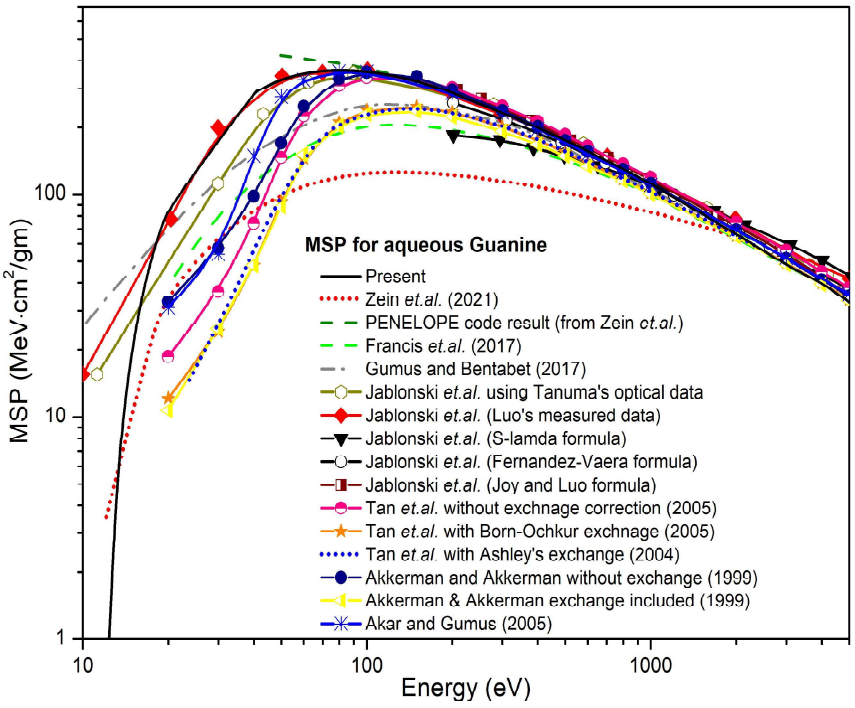

Figure 5.24 MSP for aqueous Guanine

Line: Present; short dot line: Zein et.al. [35]; olive green dash: PENELOPE code [35]; dash line: Francis et.al. [48]; gray dash dot: Gümüş and Bentabet [47]; open hexagons: Jablonski et.al. using optical data [44]; diamonds: measured by Luo taken from Joy's database [44]; inverted triangles: S-lamda approach [44]; open circles: Fernández-Varea formula [44]; half-filled squares: Joy and Luo formula [44]; blue dot line: Tan et.al. with Ashley exchange [34]; half-filled circles: Tan et.al. without exchange [30]; filled stars: Tan et.al. with Born-Ochkur exchange [30]; half-filled triangles: Akkerman and Akkerman with Ashley exchange [36]; solid circles: Akkerman and Akkerman without exchange [36];

asterisk: Akar and Gümüş [45]

The present computed results of electron MSP for aqueous Guanine are plotted in the figure 5.24. Using the mentioned density (Table 5.5), we converted the SP values provided by Akkerman and Akkerman [36], Jablonski *et.al.* [44], Tan *et.al.* [30] into mass stopping power, MSP. Jablonski *et.al.* [44] provided the SP values for energy beyond 200 eV using three different formulas, namely the S-lamda approach [44], Joy and Luo formula [49] and Fernández-Varea formula [50]. They also provided Luo's measured SP values from Joy's database [56]and computed SP utilising Tanuma *et. al.* optical data in a dielectric response theory-based computation. All of these SP values were estimated roughly by adding the SP of the solid's atomic constituents with weights obtained by mass fractions. According to Jablonski *et.al.* [44], the predicted SP between 10-100 eV energy range is less accurate than those for higher energies. Therefore, it was expected that their data at lower energy regimes would deviate from the present MSP values. However, for energies above 20 eV, the current results overlap with Luo's measured data [44]. Beyond 50 eV, the present results are observed to be in an excellent agreement with all the reported data of Jablonski *et.al.* [44], Akkerman and Akkerman data without exchange [36], Tan *et.al.* results without exchange correction [30], Akar and Gümüş [45] data and the results of the PENELOPE code simulations [35].

Figure 5.25 depicts a plot of present computed electron MSP data for an aqueous Thymine molecule with available comparisons [30,35,45,48]. Tan *et.al.* [30] results with Born-Ochkur correction indicate lower MSP values, as previously observed. However, there is a very strong agreement between the present results and the data of Tan *et.al.* [30] without exchange correction, PENELOPE code simulation findings [35] and data of Akar and Gümüş [45]. While the current curve's behaviour with the reported data of Zein *et.al.* [35] reveals a similar pattern. The mutual divergence is observed at lower energy side, particularly.

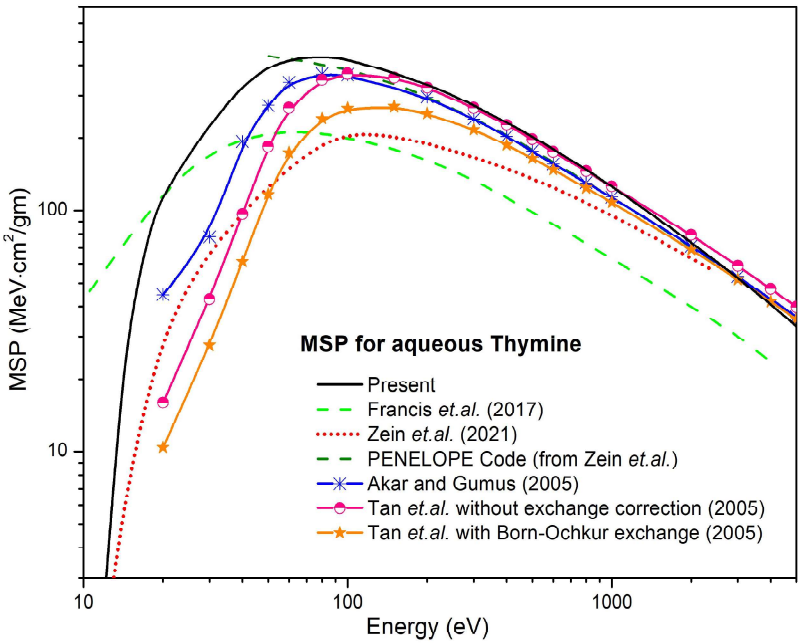

Figure 5.25 MSP for aqueous Thymine

Line: Present; green dash: Francis et. al. [48]; red dot line: Zein et. al. [35]; olive green dash line: PENELOPE code [35]; asterisk: Akar and Gümüş [45]; half-filled circles: Tan et. al. without exchange [30]; filled stars: Tan et. al. with Born-Ochkur exchange [30]

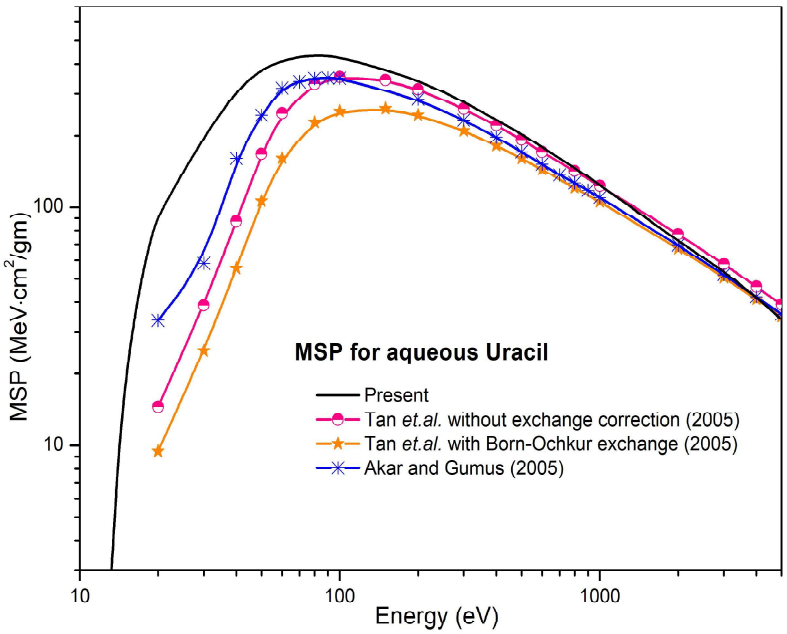

Figure 5.26 MSP for aqueous Uracil

Line: Present; half-filled circles: Tan et.al. without exchange [30]; filled stars: Tan et.al. with Born-Ochkur exchange [30]; asterisk: Akar and Gümüş [45]

The current MSP values for the aqueous uracil molecule are displayed in figure 5.26. Tan *et.al.* [30] reported the results with and without Born-Ochkur exchange effect. Akar and Gümüş [45] used the generalised oscillator strength (GOS) model to report the SP data.

As previously pointed out, the collisional SP data of Akar and Gümüş [45] for all studied DNA constituent molecules were converted into MSP by taking density of the medium into account (Table 5.5). It is worth noting here that the total SP includes collisional SP and bremsstrahlung SP [46]. However, bremsstrahlung SP is only important above 300 keV energy. Collisional SP data have therefore been used for the comparison for all the molecules under investigation in the present study, where the energy range is from the threshold energy to 5000 eV.

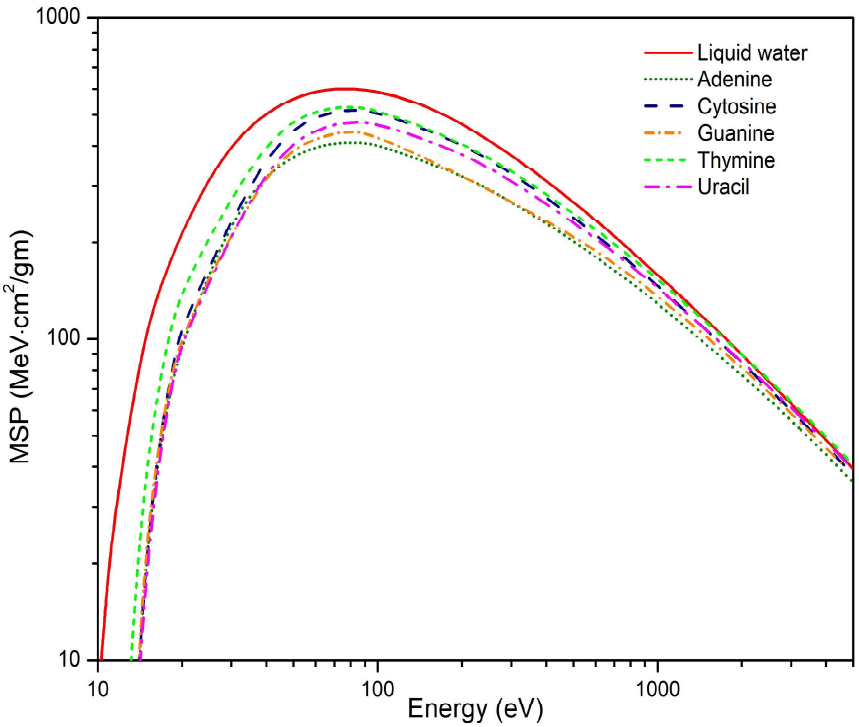

Figure 5.27 Present MSP for DNA molecules and liquid water

Figure 5.27 depicts a comparison of the MSP data of DNA molecules and that of liquid water (estimated by us from the IMFP data of Nidhi Sinha and Bobby Antony ([38]). Because water has a lower density (0.997 gm/cm^3) than DNA constituents (Table 5.5), the MSP ($= SP/\rho$) of liquid water is expected to be greater than that of DNA constituents, as shown in figure 5.27.

As a result of all the approximations involved in the present computations, the valley region of inelastic mean free path, which is located at around 80–100 eV, is experienced an uncertainty of 10–15%. In this energy spectrum, the mass stopping power has an equivalent influence. These uncertainties are smaller at lower energies and steadily decrease above 100 eV.

5.5 Absorbed Dose (D)

"Absorbed dose (D)" is a measurement that shows how much energy, a unit mass of a material absorbs. It is a general phrase that refers to any type of radiation or material that is utilised in radiobiology, since it is an excellent tool to forecast the harm that a specific type of

radiation would do to an organ [57]. The absorbed dose for each of the five components of DNA is also provided in the present study. This is the first attempt to report absorbed dose results for the aqueous compounds currently under investigation.

5.5.1 Results and Discussion

In addition to IMFP and MSP, we also calculated the absorbed dosage (D), for all the compounds under investigation. Figures 5.28 to 5.32 show three-dimensional graphs of the absorbed dose (D) vs incident energy (E_i) and distance (r) for the present studied aqueous DNA constituents. The displayed energy values are in the $log_{10}(E_i)$ scale.

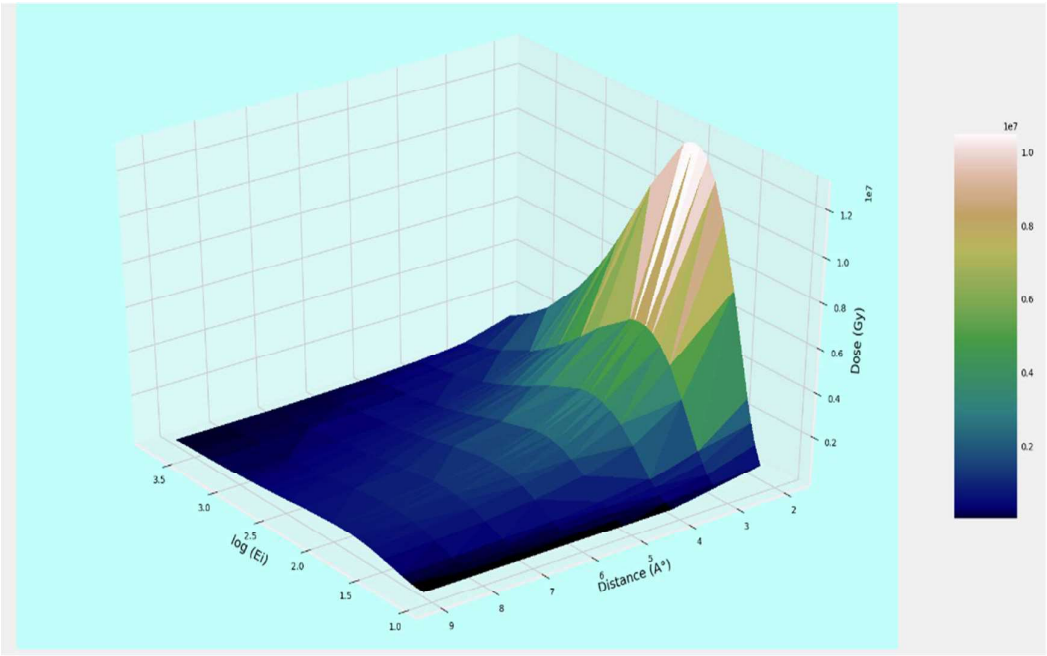

Figure 5.28 3D plot of absorbed dose for Adenine

The absorption of energy in the target medium starts as soon as the projectile energy of the incident electrons exceeds the value $\Delta = I + E_{gap}$, and it reaches its maximum value, as indicated by the peak of Q_{inel}, at roughly $80 - 90$ eV. Maximum energy transfers, and thus the peak of dosage absorption, happen at this energy. Furthermore, the inverse dependency of the absorbed dose to the distance helps to explain how it decreases over distance.

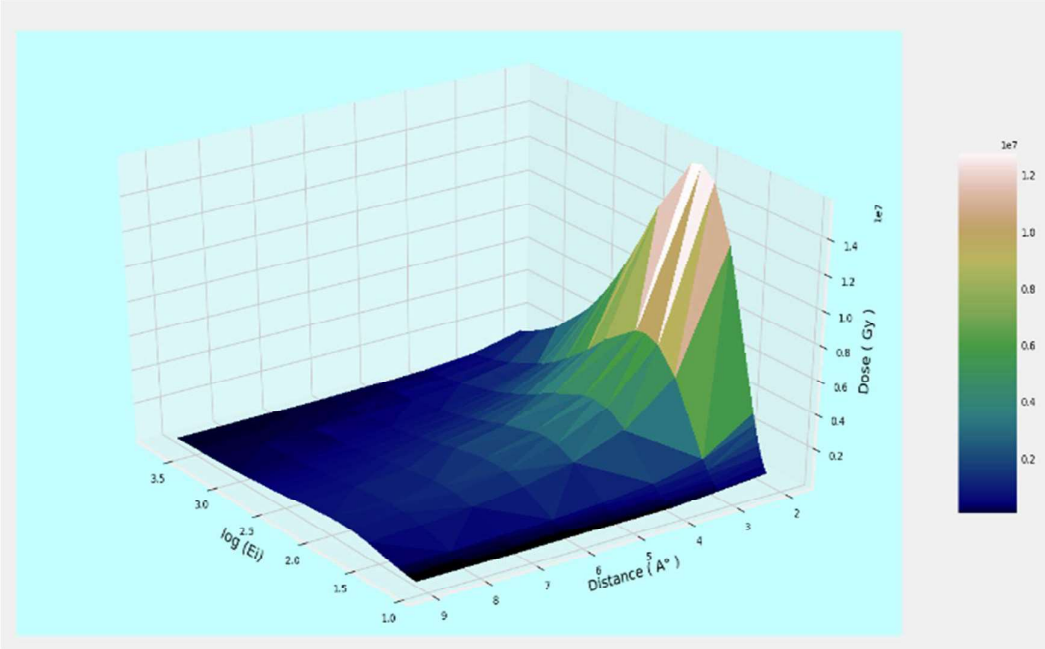

Figure 5.29 3D plot of absorbed dose for Cytosine

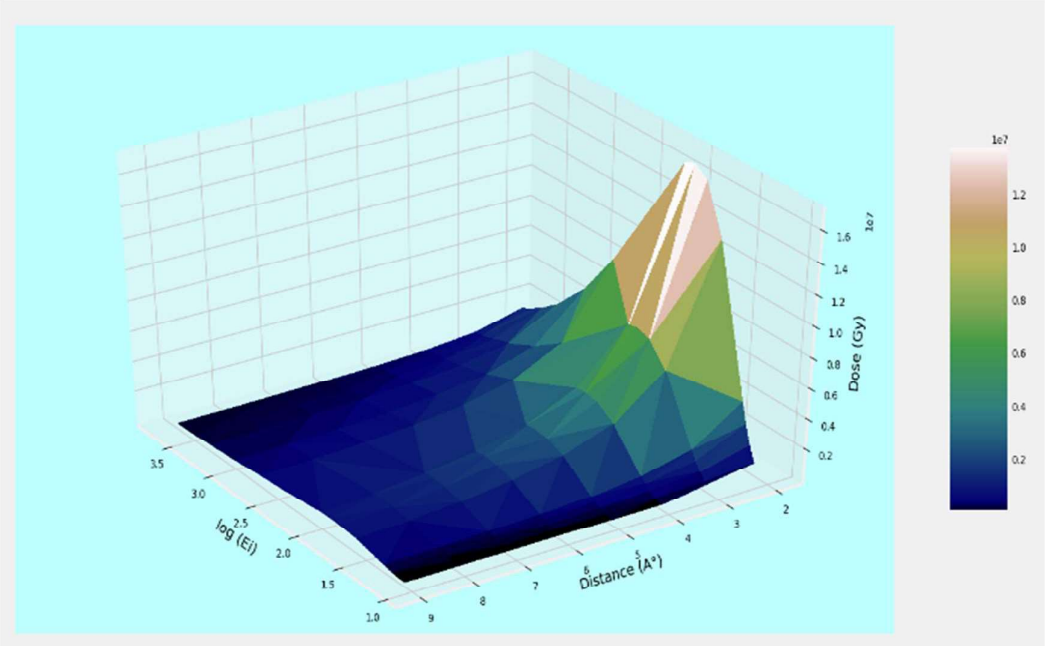

Figure 5.30 3D plot of Absorbed Dose for Guanine

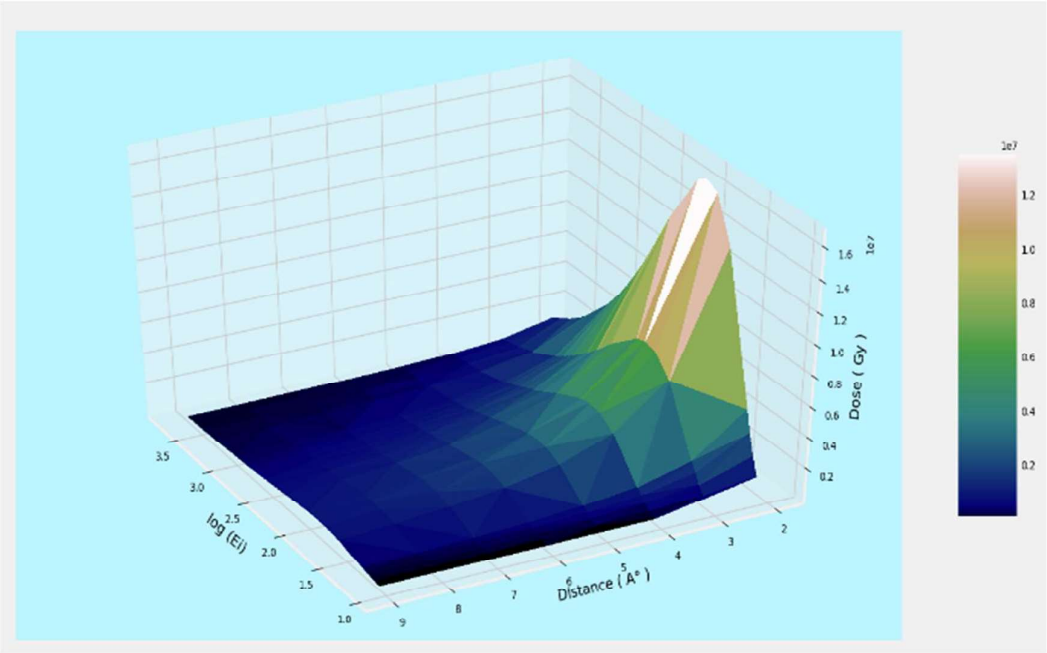

Figure 5.31 3D plot of absorbed dose for Thymine

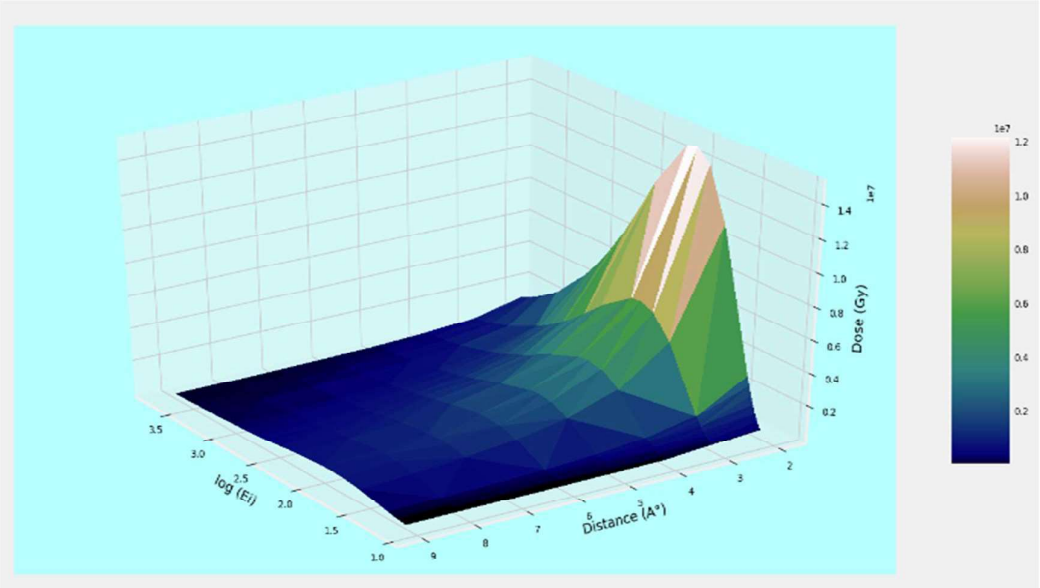

Figure 5.32 3D plot of absorbed dose for Uracil

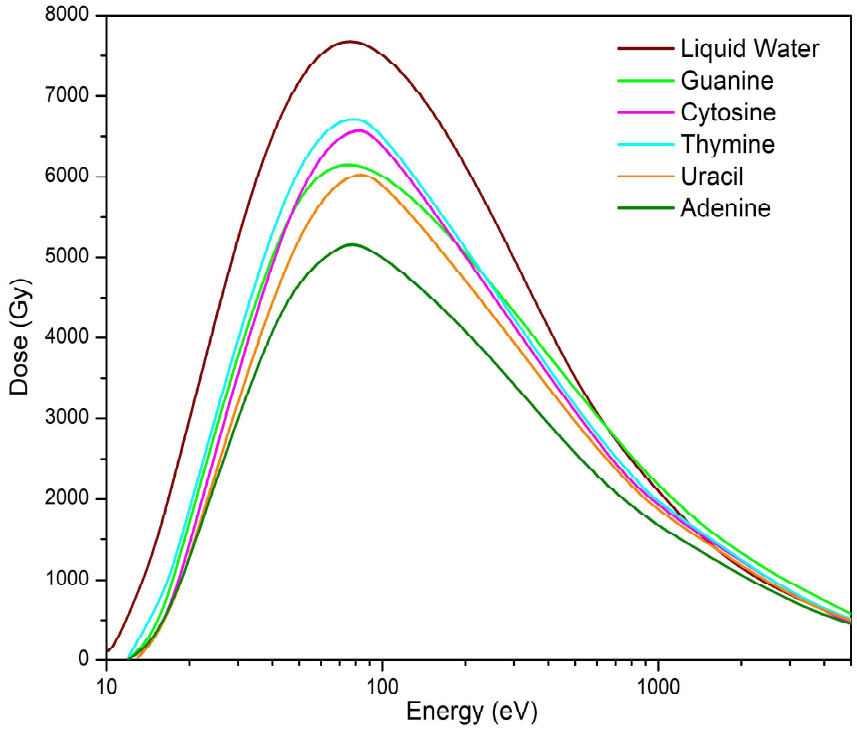

Figure 5.33 Dose vs Energy plot for DNA molecules and liquid water at distance r = 100 Å

The absorbed dose vs. energy curve for the present DNA molecules at the specified distance, r = 100 Å, is depicted in figure 5.33. We computed the absorbed dose of liquid water for comparison in order to gain a better understanding since we have studied these DNA constituents in aqueous phase. Figure 5.33 compares the absorbed doses for five DNA compunds and liquid water across a specific distance, r = 100 Å.

As can be observed from the figure 5.33, liquid water has the highest dosage value, which indicates that it absorbs the most energy when compared to the components of DNA. It is also mentioned by Elahe Alizadeh and Leon Sanche [60] that water molecules absorb roughly ~66% of the radiation energy. The IMFP values of Nidhi Sinha and Bobby Antony [38] are used in the current computation for the dosage values of the liquid water.

5.6 Bibliography

[1] J. B. Little, *Radiation Carcinogenesis*, Carcinogenesis **21**, 397 (2000).

[2] A. K. Basu, *DNA Damage, Mutagenesis and Cancer*, Int J Mol Sci **19**, (2018).

[3] H. Nikjoo, R. Taleei, T. Liamsuwan, D. Liljequist, and D. Emfietzoglou, *Perspectives in Radiation Biophysics: From Radiation Track Structure Simulation to Mechanistic Models of DNA Damage and Repair*, Radiation Physics and Chemistry **128**, 3 (2016).

[4] D. T. Goodhead, *Initial Events in the Cellular Effects of Ionizing Radiations: Clustered Damage in DNA*, Int J Radiat Biol **65**, 7 (1994).

[5] J. A. Laverne and S. M. Pimblott, Electron Energy-Loss Distributions in Solid, Dry DNA, 1995.

[6] Z. Tan, Y. Xia, M. Zhao, and X. Liu, *Electron Stopping Power and Inelastic Mean Free Path in Amino Acids and Protein over the Energy Range of 20-20,000 EV*, Radiat Environ Biophys **45**, 135 (2006).

[7] Maurizio Dapor, *Transport of Energetic Electrons in Solids: Computer Simulation with Applications to Materials Analysis and Characterization* (2014).

[8] R. Garcia-Molina, I. Abril, I. Kyriakou, and D. Emfietzoglou, *Inelastic Scattering and Energy Loss of Swift Electron Beams in Biologically Relevant Materials*, Surface and Interface Analysis **49**, 11 (2017).

[9] H. Khesbak, O. Savchuk, S. Tsushima, and K. Fahmy, *The Role of Water H-Bond Imbalances in B-DNA Substate Transitions and Peptide Recognition Revealed by Time-Resolved FTIR Spectroscopy*, J Am Chem Soc **133**, 5834 (2011).

[10] Helmholtz Association of German Research Centres, *Water Molecules Characterize the Structure of DNA Genetic Material.*, https://www.sciencedaily.com/releases/2011/04/110426091122.htm#citation_apa.

[11] Z. Tan, Y. Xia, X. Liu, M. Zhao, Y. Ji, F. Li, and B. Huang, *Cross Sections of Electron Inelastic Interactions in DNA*, Radiat Environ Biophys **43**, 173 (2004).

[12] H. Q. Tan, Z. Mi, and A. A. Bettiol, *Simple and Universal Model for Electron-Impact Ionization of Complex Biomolecules*, Phys Rev E **97**, 1 (2018).

[13] P. De Vera, I. Abril, and R. Garcia-Molina, *Excitation and Ionisation Cross-Sections in Condensed-Phase Biomaterials by Electrons down to Very Low Energy: Application to Liquid Water and Genetic Building Blocks*, Physical Chemistry Chemical Physics **23**, 5079 (2021).

[14] C. E. Crespo-Hernández, R. Arce, Y. Ishikawa, L. Gorb, J. Leszczynski, and D. M. Close, *Ab Initio Ionization Energy Thresholds of DNA and RNA Bases in Gas Phase and in Aqueous Solution*, Journal of Physical Chemistry A **108**, 6373 (2004).

[15] H. Fernando, G. A. Papadantonakis, N. S. Kim, and P. R. Lebreton, *Conduction-Band-Edge Ionization Thresholds of DNA Components in Aqueous Solution*, Proc Natl Acad Sci U S A **95**, 5550 (1998).

[16] S. Gop, R. Sutradhar, S. Chakraborty, and T. P. Sinha, *The Study of Energetic and Electronic Properties of Metal-Adenine Complex in Solvent Phase: A Density Functional Theory Approach*, in *AIP Conference Proceedings*, Vol. 2162 (American Institute of Physics Inc., 2019).

[17] M. T. Baei, M. R. Taghartapeh, E. T. Lemeski, and A. Soltani, *A Computational Study of Adenine, Uracil, and Cytosine Adsorption upon AlN and BN Nano-Cages*, Physica B Condens Matter **444**, 6 (2014).

[18] R. di Felice, A. Calzolari, E. Molinari, and A. Garbesi, *Ab Initio Study of Model Guanine Assemblies: The Role of (Formula Presented) Coupling and Band Transport*, Phys Rev B Condens Matter Mater Phys **65**, 1 (2002).

[19] J. MacNaughton, A. Moewes, and E. Z. Kurmaev, *Electronic Structure of the Nucleobases*, Journal of Physical Chemistry B **109**, 7749 (2005).

[20] P. W. Harland and C. Vallance, *Ionization Cross-Sections and Ionization Efficiency Curves from Polarizability Volumes and Ionization Potentials*, Int J Mass Spectrom Ion Process **171**, 173 (1997).

[21] S. Nakagawa, *Polarizable Model Potential Function for Nucleic Acid Bases*, J Comput Chem **28**, 1538 (2007).

[22] L. Onsager, *Electric Moments of Molecules in Liquids*, J Am Chem Soc **58**, 1486 (1936).

[23] M. Valiskó and D. Boda, *Dielectric Constant of the Polarizable Dipolar Hard Sphere Fluid Studied by Monte Carlo Simulation and Theories*, Condens Matter Phys **8**, 357 (2005).

[24] P. Szarek, *Electric Permittivity in Individual Atomic and Molecular Systems Through Direct Associations with Electric Dipole Polarizability and Chemical Hardness*, Journal of Physical Chemistry C **121**, 12593 (2017).

[25] D. Emfietzoglou, K. Karava, G. Papamichael, and M. Moscovitch, *Monte Carlo Simulation of the Energy Loss of Low-Energy Electrons in Liquid Water*, Phys Med Biol **48**, 2355 (2003).

[26] H. Nikjoo, H. Nikjoo, S. Uehara, I. G. Khvostunov, F. A. Cucinotta, W. E. Wilson, and D. T. Goodhead, *Monte Carlo Track Structure for Radiation Biology and Space Applications*, Physica Medica **17**, 38-44 (2001).

[27] W. Friedland, P. Jacob, H. G. Paretzke, and T. Stork, *Monte Carlo Simulation of the Production of Short DNA Fragments by Low-Linear Energy Transfer Radiation Using Higher-Order DNA Models*, Radiat Res **150**, 170 (1998).

[28] H. Nikjoo, S. Uehara, W. E. Wilson, M. Hoshi, and D. T. Goodhead, *Track Structure in Radiation Biology: Theory and Applications*, Int J Radiat Biol **73**, 355 (1998).

[29] M. A. Flores-Mancera, J. S. Villarrubia, and G. Massillon-Jl, *Electron Inelastic Mean Free Paths for LiF, CaF2, Al2O3, and Liquid Water from 433 KeV down to the Energy Gap*, ACS Omega **5**, 4139 (2020).

[30] Z. Tan, Y. Xia, X. Liu, M. Zhao, Y. Ji, F. Li, and B. Huang, *Electron Inelastic Interactions in Bioorganic Compounds in the Energy Range of 20-10000 EV*, Appl Phys A Mater Sci Process **81**, 779 (2005).

[31] S. Tanuma, C. J. Powell, and D. R. Penn, *Calculations of Electron Inelastic Mean Free Paths. V. Data for 14 Organic Compounds over the 50–2000 EV Range*, Surface and Interface Analysis **21**, 165 (1994).

[32] A. Akar, H. Gümüş, and N. T. Okumuşoğlu, *Electron Inelastic Mean Free Path Formula and CSDA-Range Calculation in Biological Compounds for Low and Intermediate Energies*, Applied Radiation and Isotopes **64**, 543 (2006).

[33] P. J. Cumpson, *Estimation of Inelastic Mean Free Paths for Polymers and Other Organic Materials: Use of Quantitative Structure-Property Relationships*, Surface and Interface Analysis **31**, 23 (2001).

[34] Z. Tan, Y. Xia, M. Zhao, X. Liu, F. Li, B. Huang, and Y. Ji, *Electron Stopping Power and Mean Free Path in Organic Compounds over the Energy Range of 20-10,000 EV*, Nucl Instrum Methods Phys Res B **222**, 27 (2004).

[35] S. A. Zein, M. C. Bordage, Z. Francis, G. Macetti, A. Genoni, C. Dal Cappello, W. G. Shin, and S. Incerti, *Electron Transport in DNA Bases: An Extension of the Geant4-DNA Monte Carlo Toolkit*, Nucl Instrum Methods Phys Res B **488**, 70 (2021).

[36] A. Akkerman and E. Akkerman, *Characteristics of Electron Inelastic Interactions in Organic Compounds and Water over the Energy Range 20-10 000 EV*, J Appl Phys **86**, (1999).

[37] D. R. Penn, *Electron Mean-Free-Path Calculations Using a Model Dielectric Function*, Phys Rev B **35**, (n.d.).

[38] N. Sinha and B. Antony, *Mean Free Paths and Cross Sections for Electron Scattering from Liquid Water*, Journal of Physical Chemistry B **125**, 5479 (2021).

[39] D. Emfietzoglou, I. Kyriakou, R. Garcia-Molina, and I. Abril, *Inelastic Mean Free Path of Low-Energy Electrons in Condensed Media: Beyond the Standard Models*, (2015).

[40] A. Muñoz, J. C. Oller, F. Blanco, J. D. Gorfinkiel, P. Limão-Vieira, and G. García, *Electron-Scattering Cross Sections and Stopping Powers in H2O*, Phys Rev A **76**, 052707 (2007).

[41] ICRU Report 37, 1937.

[42] F. Salvat, J. M. Fernández-Varea, J. Sempau and J. Mazurier , *Practical Aspects of Monte Carlo Simulation of Charged Particle Transport:Mixed Algorithms and Variance Reduction Techniques*, Radiation Environment Biophysics **38**, 15 (1999).

[43] J. Sempau, P. Andreo, J. Aldana, J. Mazurier, and F. Salvat, *Electron Beam Quality Correction Factors for Plane-Parallel Ionization Chambers: Monte Carlo Calculations Using the PENELOPE System*, Phys Med Biol **49**, 4427 (2004).

[44] A. Jablonski, S. Tanuma, and C. J. Powell, *A Predictive Formula for the Electron Stopping Power*, Journal of Surface Analysis **13**, 170 (2006).

[45] A. Akar and H. Gümüş, *Electron Stopping Power in Biological Compounds for Low and Intermediate Energies with the Generalized Oscillator Strength (GOS) Model*, Radiation Physics and Chemistry **73**, 196 (2005).

[46] A. Akar, H. Gümüş, and N. T. Okumuşoğlu, *Total Electron Stopping Powers and CSDA-Ranges from 20 EV to 10 MeV Electron Energies for Components of DNA and RNA*, Advances in Quantum Chemistry **52**, 277 (2007).

[47] H. Gümüş and A. Bentabet, *CSDA Range, Stopping Power and Mean Penetration Depth Energy Relationships in Some Hydrocarbons and Biologic Materials for 10 EV to 100 MeV with the Modified Rohrlich–Carlson Model*, Appl Phys A Mater Sci Process **123**, (2017).

[48] Z. Francis, Z. El Bitar, S. Incerti, M. A. Bernal, M. Karamitros, and H. N. Tran, *Calculation of Lineal Energies for Water and DNA Bases Using the Rudd Model Cross Sections Integrated within the Geant4-DNA Processes*, J Appl Phys **122**, 014701 (2017).

[49] D. C. Joy and S. Luo, Scanning **11**, 176 (1989).

[50] J. M. Fernandez-Varea, R. Mayol, D. Liljequist, and F. Salvat, *Inelastic Scattering of Electrons in Solids from a Generalized Oscillator Strength Model Using Optical and Photoelectric Data*, Journal of Physics: Condensed Matter **5**, 3593 (1993).

[51] N. Y. Aouina and Z. E. A. Chaoui, *Simulation of Positron and Electron Elastic Mean Free Path and Diffusion Angle on DNA Nucleobases from 10 EV to 100 KeV*, Surface and Interface Analysis **50**, 939 (2018).

[52] L. N. Trujillo-López, C. Martínez-Flores, and R. Cabrera-Trujillo, *Universal Scaling Behavior of Molecular Electronic Stopping Cross Section for Protons Colliding with Small Molecules and Nucleobases*, Nucl Instrum Methods Phys Res B **313**, 5 (2013).

[53] K. Wiklund, J. M. Fernández-Varea, and B. K. Lind, *A Monte Carlo Program for the Analysis of Low-Energy Electron Tracks in Liquid Water*, Phys Med Biol **56**, 1985 (2011).

[54] H. Gümüş and F. Köksal, *Effective Stopping Charges and Stopping Power Calculations for Heavy Ions*, Radiation Effects and Defects in Solids **157**, 445 (2002).

[55] H. Gümüş, *Simple Stopping Power Formula for Low and Intermediate Energy Electrons*, Radiation Physics and Chemistry **72**, 7 (2005).

[56] D. C. Joy, A Database of Electron-Solid Interactions, 2004.

[57] Ahmed Meghzifene, David R. Dance, Donald McLean, and Hans-Michael Kramer, *Dosimetry in Diagnostic Radiology*, Eur J Radiol **76**, 11 (2010).

[58] William V. Prestwich, Josane Nunes and Cheuk S. Kwok, *Beta Dose Point Kernels for Radionucides of Potential Use in Radioimmunotherapy*, The Journal of Nuclear Medicine **30**, 1036 (1989).

[59] Sh. Mohammed, A. Trabelsi, and K. Manai, *Stopping Power, CSDA Range, Absorbed Dose and Cross Sections Calculations of F18 Simulated in Water Using Geant4 Code*, Indian J Sci Technol **11**, 1 (2018).

[60] E. Alizadeh and L. Sanche, *Precursors of Solvated Electrons in Radiobiological Physics and Chemistry*, Chem Rev **112**, 5578 (2012).